EUROPEAN ORGANISATION FOR PARTICLE PHYSICS

CERN-PPE/93-106
21 June 1993

Measurements of B^0-$\bar{B}^0$ mixing, $\Gamma(Z^0 \to b\bar{b})/\Gamma(Z^0 \to \text{hadrons})$ and semileptonic branching ratios for b-flavoured hadrons in hadronic Z^0 decays

The OPAL Collaboration

Abstract

From a sample of about 450 000 hadronic Z^0 decays, measurements of the average B^0-$\bar{B}^0$ mixing parameter, χ, the branching fraction of Z^0 bosons into hadrons containing bottom quarks, $\Gamma(Z^0 \to b\bar{b})/\Gamma(Z^0 \to \text{hadrons})$, the average semileptonic branching ratios for such hadrons, $B(b \to \ell)$ and $B(b \to c \to \ell)$, and the mean scaled energy of these hadrons, $\langle x_E \rangle$, are presented. The measurements were obtained using a simultaneous fit to single-lepton and dilepton events collected with the OPAL detector at LEP, including both electrons and muons. The results are

$$\begin{aligned} \chi &= 0.143^{+0.022}_{-0.021} \pm 0.007 \\ \Gamma(Z^0 \to b\bar{b})/\Gamma(Z^0 \to \text{hadrons}) &= 0.222 \pm 0.011 \pm 0.007 \\ B(b \to \ell) &= (10.5 \pm 0.6 \pm 0.5)\% \\ B(b \to c \to \ell) &= (7.7 \pm 0.4 \pm 0.7)\% \\ \langle x_E \rangle &= 0.697 \pm 0.006 \pm 0.011 \end{aligned}$$

where the errors are statistical and systematic, respectively, in each case. The result for $B(b \to c \to \ell)$ excludes decays of the type $b \to \bar{c} \to \ell$.

(Submitted to Z. Phys. C)

The OPAL Collaboration

R. Akers[16], G. Alexander[23], J. Allison[16], K.J. Anderson[9], S. Arcelli[2], A. Astbury[28], D. Axen[29], G. Azuelos[18,a], J.T.M. Baines[16], A.H. Ball[17], J. Banks[16], R.J. Barlow[16], S. Barnett[16], R. Bartoldus[3], J.R. Batley[5], G. Beaudoin[18], A. Beck[23], G.A. Beck[13], J. Becker[10], C. Beeston[16], T. Behnke[27], K.W. Bell[20], G. Bella[23], P. Bentkowski[18], P. Berlich[10], S. Bethke[11], O. Biebel[3], I.J. Bloodworth[1], P. Bock[11], B. Boden[3], H.M. Bosch[11], M. Boutemeur[18], H. Breuker[8,b], P. Bright-Thomas[25], R.M. Brown[20], A. Buijs[8], H.J. Burckhart[8], C. Burgard[27], P. Capiluppi[2], R.K. Carnegie[6], A.A. Carter[13], J.R. Carter[5], C.Y. Chang[17], D.G. Charlton[8], S.L. Chu[4], P.E.L. Clarke[15], J.C. Clayton[1], I. Cohen[23], J.E. Conboy[15], M. Cooper[22], M. Coupland[14], M. Cuffiani[2], S. Dado[22], G.M. Dallavalle[2], S. De Jong[13], L.A. del Pozo[5], H. Deng[17], A. Dieckmann[11], M. Dittmar[4], M.S. Dixit[7], E. do Couto e Silva[12], J.E. Duboscq[8], E. Duchovni[26], G. Duckeck[11], I.P. Duerdoth[16], D.J.P. Dumas[6], P.A. Elcombe[5], P.G. Estabrooks[6], E. Etzion[23], H.G. Evans[9], F. Fabbri[2], B. Fabbro[21], M. Fierro[2], M. Fincke-Keeler[28], H.M. Fischer[3], D.G. Fong[17], M. Foucher[17], A. Gaidot[21], J.W. Gary[4], J. Gascon[18], N.I. Geddes[20], C. Geich-Gimbel[3], S.W. Gensler[9], F.X. Gentit[21], G. Giacomelli[2], R. Giacomelli[2], V. Gibson[5], W.R. Gibson[13], J.D. Gillies[20], J. Goldberg[22], D.M. Gingrich[30,a], M.J. Goodrick[5], W. Gorn[4], C. Grandi[2], F.C. Grant[5], J. Hagemann[27], G.G. Hanson[12], M. Hansroul[8], C.K. Hargrove[7], P.F. Harrison[13], J. Hart[8], P.M. Hattersley[1], M. Hauschild[8], C.M. Hawkes[8], E. Heflin[4], R.J. Hemingway[6], G. Herten[10], R.D. Heuer[8], J.C. Hill[5], S.J. Hillier[8], T. Hilse[10], D.A. Hinshaw[18], J.D. Hobbs[8], P.R. Hobson[25], D. Hochman[26], R.J. Homer[1], A.K. Honma[28,a], R.E. Hughes-Jones[16], R. Humbert[10], P. Igo-Kemenes[11], H. Ihssen[11], D.C. Imrie[25], A.C. Janissen[6], A. Jawahery[17], P.W. Jeffreys[20], H. Jeremie[18], M. Jimack[1], M. Jones[29], R.W.L. Jones[8], P. Jovanovic[1], C. Jui[4], D. Karlen[6], K. Kawagoe[24], T. Kawamoto[24], R.K. Keeler[28], R.G. Kellogg[17], B.W. Kennedy[15], J. King[13], S. Kluth[5], T. Kobayashi[24], D.S. Koetke[8], T.P. Kokott[3], S. Komamiya[24], J.F. Kral[8], R. Kowalewski[8], J. von Krogh[11], J. Kroll[9], P. Kyberd[13], G.D. Lafferty[16], H. Lafoux[21], R. Lahmann[17], F. Lamarche[18], J. Lauber[8], J.G. Layter[4], P. Leblanc[18], A.M. Lee[31], E. Lefebvre[18], M.H. Lehto[15], D. Lellouch[26], C. Leroy[18], J. Letts[4], L. Levinson[26], S.L. Lloyd[13], F.K. Loebinger[16], J.M. Lorah[17], B. Lorazo[18], M.J. Losty[7], X.C. Lou[12], J. Ludwig[10], A. Luig[10], M. Mannelli[8], S. Marcellini[2], C. Markus[3], A.J. Martin[13], J.P. Martin[18], T. Mashimo[24], P. Mättig[3], U. Maur[3], J. McKenna[29], T.J. McMahon[1], J.R. McNutt[25], F. Meijers[8], D. Menszner[11], F.S. Merritt[9], H. Mes[7], A. Michelini[8], R.P. Middleton[20], G. Mikenberg[26], J. Mildenberger[6], D.J. Miller[15], R. Mir[12], W. Mohr[10], C. Moisan[18], A. Montanari[2], T. Mori[24], M. Morii[24], U. Müller[3], B. Nellen[3], H.H. Nguyen[9], S.W. O'Neale[1], F.G. Oakham[7], F. Odorici[2], H.O. Ogren[12], C.J. Oram[28,a], M.J. Oreglia[9], S. Orito[24], J.P. Pansart[21], B. Panzer-Steindel[8], P. Paschievici[26], G.N. Patrick[20], N. Paz-Jaoshvili[23], M.J. Pearce[1], P. Pfister[10], J.E. Pilcher[9], J. Pinfold[30], D. Pitman[28], D.E. Plane[8], P. Poffenberger[28], B. Poli[2], T.W. Pritchard[13], H. Przysiezniak[18], G. Quast[27], M.W. Redmond[8], D.L. Rees[8], G.E. Richards[16], M. Rison[5], S.A. Robins[5], D. Robinson[8], A. Rollnik[3], J.M. Roney[28,c], E. Ros[8], S. Rossberg[10], A.M. Rossi[2], M. Rosvick[28], P. Routenburg[30], K. Runge[10], O. Runolfsson[8], D.R. Rust[12], M. Sasaki[24], C. Sbarra[2], A.D. Schaile[26], O. Schaile[10], W. Schappert[6], F. Scharf[3], P. Scharff-Hansen[8], P. Schenk[4], B. Schmitt[3], H. von der Schmitt[11], M. Schröder[12], C. Schwick[27], J. Schwiening[3], W.G. Scott[20], M. Settles[12], T.G. Shears[5], B.C. Shen[4], C.H. Shepherd-Themistocleous[7], P. Sherwood[15], G.P. Siroli[2], A. Skillman[16], A. Skuja[17], A.M. Smith[8], T.J. Smith[28], G.A. Snow[17], R. Sobie[28,b],

R.W. Springer[17], M. Sproston[20], A. Stahl[3], C. Stegmann[10], K. Stephens[16], J. Steuerer[28], R. Ströhmer[11], D. Strom[19], H. Takeda[24], T. Takeshita[24,d], S. Tarem[26], M. Tecchio[9], P. Teixeira-Dias[11], N. Tesch[3], M.A. Thomson[15], E. Torrente-Lujan[22], S. Towers[28], G. Transtromer[25], N.J. Tresilian[16], T. Tsukamoto[24], M.F. Turner[8], D. Van den plas[18], R. Van Kooten[27], G.J. VanDalen[4], G. Vasseur[21], A. Wagner[27], D.L. Wagner[9], C. Wahl[10], C.P. Ward[5], D.R. Ward[5], P.M. Watkins[1], A.T. Watson[1], N.K. Watson[8], M. Weber[11], P. Weber[6], P.S. Wells[8], N. Wermes[3], M.A. Whalley[1], B. Wilkens[10], G.W. Wilson[4], J.A. Wilson[1], V-H. Winterer[10], T. Wlodek[26], G. Wolf[26], S. Wotton[11], T.R. Wyatt[16], R. Yaari[26], A. Yeaman[13], G. Yekutieli[26], M. Yurko[18], W. Zeuner[8], G.T. Zorn[17].

[1]School of Physics and Space Research, University of Birmingham, Birmingham, B15 2TT, UK
[2]Dipartimento di Fisica dell' Università di Bologna and INFN, Bologna, 40126, Italy
[3]Physikalisches Institut, Universität Bonn, D-5300 Bonn 1, Germany
[4]Department of Physics, University of California, Riverside, CA 92521 USA
[5]Cavendish Laboratory, Cambridge, CB3 0HE, UK
[6]Carleton University, Dept of Physics, Colonel By Drive, Ottawa, Ontario K1S 5B6, Canada
[7]Centre for Research in Particle Physics, Carleton University, Ottawa, Ontario K1S 5B6, Canada
[8]CERN, European Organisation for Particle Physics, 1211 Geneva 23, Switzerland
[9]Enrico Fermi Institute and Dept of Physics, University of Chicago, Chicago Illinois 60637, USA
[10]Fakultät für Physik, Albert Ludwigs Universität, D-7800 Freiburg, Germany
[11]Physikalisches Institut, Universität Heidelberg, Heidelberg, Germany
[12]Indiana University, Dept of Physics, Swain Hall West 117, Bloomington, Indiana 47405, USA
[13]Queen Mary and Westfield College, University of London, London, E1 4NS, UK
[14]Birkbeck College, London, WC1E 7HV, UK
[15]University College London, London, WC1E 6BT, UK
[16]Department of Physics, Schuster Laboratory, The University, Manchester, M13 9PL, UK
[17]Department of Physics, University of Maryland, College Park, Maryland 20742, USA
[18]Laboratoire de Physique Nucléaire, Université de Montréal, Montréal, Quebec, H3C 3J7, Canada
[19]University of Oregon, Dept of Physics, Eugene, Oregon 97403, USA
[20]Rutherford Appleton Laboratory, Chilton, Didcot, Oxfordshire, OX11 0QX, UK
[21]DAPNIA/SPP, Saclay, F-91191 Gif-sur-Yvette, France
[22]Department of Physics, Technion-Israel Institute of Technology, Haifa 32000, Israel
[23]Department of Physics and Astronomy, Tel Aviv University, Tel Aviv 69978, Israel
[24]International Centre for Elementary Particle Physics and Dept of Physics, University of Tokyo, Tokyo 113, and Kobe University, Kobe 657, Japan
[25]Brunel University, Uxbridge, Middlesex, UB8 3PH UK
[26]Nuclear Physics Department, Weizmann Institute of Science, Rehovot, 76100, Israel
[27]Universität Hamburg/DESY, II Inst für Experimental Physik, 2000 Hamburg 52, Germany
[28]University of Victoria, Dept of Physics, P O Box 3055, Victoria BC V8W 3P6, Canada
[29]University of British Columbia, Dept of Physics, Vancouver BC V6T 1Z1, Canada
[30]University of Alberta, Dept of Physics, Edmonton AB T6G 2N5, Canada
[31]Duke University, Dept of Physics, Durham, North Carolina 27708-0305, USA

[a] Also at TRIUMF, Vancouver, Canada V6T 2A3
[b] Now at MPI, München, Germany
[c] And IPP, University of Victoria, Dept of Physics, P O Box 3055, Victoria BC V8W 3P6, Canada
[d] Also at Shinshu University, Matsumoto 390, Japan

1 Introduction

The identification of leptons in hadronic Z^0 decays produced through e^+e^- annihilation provides an opportunity to measure several properties of b quarks and b-flavoured hadrons, including the neutral-current coupling to b quarks, the mean scaled energy of b-flavoured hadrons, B^0-$\bar{B}^0$ mixing[1], and the semileptonic branching ratios of b-flavoured hadrons, thus probing the electroweak and strong interactions of the standard model.

The transformation of a neutral meson into its antiparticle is made possible by flavour-changing weak interactions. In the standard model, the dominant contribution to mixing in the B^0-$\bar{B}^0$ system arises from box diagrams involving virtual top quarks [1]. In Z^0 decays, both B_s^0 and B_d^0 mesons are thought to be produced in addition to charged B mesons and b-flavoured baryons. The overall rate of mixing in these events should therefore depend on the Cabbibo-Kobayashi-Maskawa matrix elements V_{td} and V_{ts} [2], and on the top-quark mass. Given that significant B_d^0 mixing has been observed by the ARGUS and CLEO collaborations in decays of the $\Upsilon(4S)$ [3, 4], where only B_d^0 and B^+ mesons are produced, and that $|V_{ts}| > |V_{td}|$ [5], B_s^0 mixing is expected to be almost full, meaning that 50% of produced B_s^0 mesons decay as $\bar{B}_s^0$ mesons and vice versa. Previous measurements [6–8] are consistent with full B_s^0 mixing. The measurement of mixing in this paper is in terms of the average mixing parameter, χ, defined as

$$\chi = \frac{B(b \to \bar{B}^0 \to B^0 \to \ell^+ X)}{B(b \to \ell^\pm X)}, \tag{1}$$

where the denominator includes all b-flavoured hadrons produced[2], and ℓ is either an electron or a muon. The relationship between χ and the parameters χ_d and χ_s, which represent the mixing probabilities in the B_d^0 and B_s^0 systems, respectively, is

$$\chi = f_d\chi_d + f_s\chi_s, \tag{2}$$

where f_d and f_s are the fractions of b-flavoured hadrons undergoing semileptonic decay that are B_d^0 and B_s^0 mesons (or $\bar{B}_d^0$, $\bar{B}_s^0$) respectively.

The partial decay widths of the Z^0 for the different quark and lepton channels are predicted by the standard model. While the leptonic partial widths and the total hadronic widths have been measured to a precision better than 1% [9, 10], the partial widths for individual quark flavours have been measured to an accuracy of only about 5% for the case of $\Gamma(Z^0 \to b\bar{b})$ [11–18] Electroweak corrections result in predictions of $\Gamma(Z^0 \to b\bar{b})$, referred to as $\Gamma_{b\bar{b}}$ throughout the rest of this paper, that depend less on the value of the top quark mass than do the predictions of the partial widths for the lighter quarks. When measured precisely, $\Gamma_{b\bar{b}}$ would thus provide an important test of the standard model. In this paper, the ratio of $\Gamma_{b\bar{b}}$ to the total hadronic width, Γ_{had}, is measured. A value of $\Gamma_{b\bar{b}}$ is obtained using the OPAL measurement of Γ_{had} [10].

Spectator model predictions for the average semileptonic branching ratio for b-flavoured hadrons, $B(b \to \ell)$, of about 12% or more [19], are significantly larger than the values below 11% which have been measured by the CLEO [20] and ARGUS [21] collaborations. Recent

[1] In this paper, B^0 refers to the mix of B_d^0 and B_s^0 produced in Z^0 decays.

[2] Reference to a b or c quark decay or to a b-flavoured or c-flavoured hadron decay is assumed to imply the charge-conjugate process for $\bar{b}$ and $\bar{c}$, and CP violation is assumed to be negligible.

predictions including non-perturbative effects give more compatible results [22]. For b-flavoured hadrons produced in Z^0 decays, $B(b \to \ell)$ receives additional contributions from B_s^0 and b-flavoured baryons, whose semileptonic branching ratios may be different. In the presence of background, uncertainty on $B(b \to \ell)$ can lead to a large systematic error in the measurement of χ [7].

The measurement of the branching fraction for the decay of b-flavoured hadrons to c-flavoured hadrons that undergo semileptonic decay, $B(b \to c \to \ell)$[3], is more of experimental than theoretical interest since predictions depend on the largely unmeasured mix of intermediate c-flavoured hadrons produced. For a decaying b quark, a lepton from $b \to c \to \ell$ decay has opposite sign from one produced through the direct decay $b \to \ell$. Thus leptons from $b \to c \to \ell$ decay form an important background for measurements of B^0-$\bar{B}^0$ mixing. By contrast, a lepton from $b \to \bar{c} \to \ell$[3] decay has the same charge sign as that of the decaying b quark, so $b \to \bar{c} \to \ell$ decay does not lead to an important background for these measurements. The use of $B(b \to c \to \ell)$ measured at lower energies [20] is unsatisfactory since corrections are necessary to account for the different mix of b-flavoured hadrons in Z^0 decays and since these previous branching-ratio measurements do not distinguish between $b \to c \to \ell$ and $b \to \bar{c} \to \ell$ decays.

The distribution of the scaled energy, x_E, of b-flavoured hadrons produced in Z^0 decays depends on the fragmentation of quarks into hadrons. Formally, $x_E = 2E_{\rm hadron}/\sqrt{s}$, where $E_{\rm hadron}$ is the energy of the first-rank hadron and $\sqrt{s}$ is the centre-of-mass energy. Predictions for such distributions depend on a convolution of perturbative QCD calculations and non-perturbative parametrisations. Precise quantitative predictions are not available. An accurate measurement of the mean scaled energy, $\langle x_E \rangle$, for b-flavoured hadrons produced in Z^0 decays reduces systematic uncertainties for any b-physics measurement relying on leptons.

Leptons from direct $b \to \ell$ decays are characterised by large components of momentum parallel and transverse to the direction of the relatively heavy b-flavoured hadron. This characteristic is used to identify event samples enriched in $b \to \ell$ decays, used here for the measurements of χ, $\Gamma_{b\bar{b}}/\Gamma_{\rm had}$, $B(b \to \ell)$ and $\langle x_E \rangle$. The rate of such events depends both on $\Gamma_{b\bar{b}}/\Gamma_{\rm had}$ and on $B(b \to \ell)$, but these two quantities can be disentangled by considering the rates of both single-lepton and dilepton events. Information on fragmentation is extracted from the momentum spectrum of the leptons. The signal for mixing is obtained from dilepton events in which both leptons arise from direct $b \to \ell$ decays and carry the same charge sign. In the absence of background, uncertainties in branching ratios and efficiencies cancel when considering the fraction of dilepton events that have the same charge sign. Events for which a b-flavoured hadron and a c-flavoured hadron in the same decay chain both decay semileptonically provide a clean signature for $b \to c \to \ell$ decays. A simultaneous fit is performed using single-lepton and dilepton distributions to determine χ, $\Gamma_{b\bar{b}}/\Gamma_{\rm had}$, $B(b \to \ell)$, $B(b \to c \to \ell)$ and $\langle x_E \rangle$.

The selection of events and the lepton identification procedures are described in Section 2. The predictions for the signal and backgrounds are explained in Sections 3 and 4. Section 5 presents the fitting procedure and results. Cross checks on the results are described in Section 6, and systematic errors are addressed in Section 7. Conclusions are given in Section 8.

[3] The b in $b \to c \to \ell$ and $b \to \bar{c} \to \ell$ refers to the decaying b quark, after any mixing has occurred.

2 Event selection

The data were recorded with the OPAL detector [23] at the CERN e^+e^- collider LEP. Tracking of charged particles is performed by a central detector, consisting of a jet chamber, a vertex detector, and z-chambers measuring the z coordinate[4] of tracks as they leave the jet chamber in the range $|\cos\theta| < 0.72$. The central detector is positioned inside a solenoidal coil, which provides a uniform magnetic field of 0.435 T. The jet chamber is a large-volume drift chamber, 4 m long and 3.7 m in diameter, divided into 24 azimuthal sectors with 159 layers of sense wires. This chamber provides measurements of the specific ionization energy loss of charged tracks, $\mathrm{d}E/\mathrm{d}x$, with excellent resolution [24]. The coil is surrounded by a time-of-flight counter array and a lead-glass electromagnetic calorimeter, divided into a cylindrical barrel and endcaps. The barrel lead-glass blocks, covering the range $|\cos\theta| < 0.82$, are arranged in an approximately projective geometry on a cylinder of radius 2.45 m. Each block has a face of 10 cm by 10 cm and a depth of about 25 radiation lengths. The magnet return yoke serves as a hadron calorimeter and is instrumented with nine layers of streamer tubes, read out onto pads and onto aluminium strips of width 4 mm. The data from the strips are used to aid muon identification. Outside the hadron calorimeter are muon chambers, which cover 93% of the full solid angle. A particle from the interaction point must traverse at least seven, and in most regions eight, interaction lengths of material to arrive at the muon chambers; thus most muons with initial momenta larger than 3 GeV/c penetrate this material.

Hadronic Z^0 decays were selected in the manner described in a previous publication [7], with centre-of-mass energies ranging between 88.2 GeV and 94.2 GeV. The mean centre-of-mass energy was 91.29 GeV for these events with an r.m.s. of 0.82 GeV, which has a negligible effect on the value of $\Gamma_{\mathrm{b\bar{b}}}/\Gamma_{\mathrm{had}}$. The jet chamber, the vertex chamber and the electromagnetic calorimeter were required to be fully operational for all events. Leptons were selected only in those events where the necessary detectors were operational, but muon detectors were not required for the selection of electrons and vice versa. Selecting events in this way made maximal use of the event statistics. This procedure led to numbers of hadronic decays available for different lepton categories which ranged from 455 344 to 480 398.

2.1 Muon identification

Tracks were considered as candidates for muons if the polar angle was in the range $|\cos\theta| < 0.95$, and the measured momentum was larger than 4 GeV/c. Below this momentum, backgrounds are fairly large.

Candidates for muons recorded in the muon chambers were identified by requiring a match between the position of an extrapolated central detector track and a track segment in the muon chambers. Candidate tracks were required to satisfy $\mathrm{d}E/\mathrm{d}x$ requirements designed to reject kaons and protons while retaining 97% of muons. Muon candidates were rejected if there were more than 20 muon segments reconstructed within an azimuthal slice of 300 mrad about the

[4]The coordinate system is defined with positive z along the e^- beam direction, θ and ϕ being the polar and azimuthal angles. The origin is taken to be the centre of the detector.

candidate segment. This selection is described in more detail elsewhere [17]. Additional criteria were required to further suppress the background, while reducing the efficiency only slightly. The separation between a matched extrapolated track and a muon segment was required to be smaller than 50% of such a separation for any other track in the event — otherwise the matched track was rejected. This requirement reduced the probability of associating the wrong central-detector track with a muon segment. Fiducial cuts were applied to remove candidates passing through known small holes in the calorimeter iron. Muon segments from pairs of muon candidates were required to be separated by at least 50 mrad, and to be inconsistent with a single muon segment for which there is an error in reconstruction. These criteria also effectively rejected pairs of candidates that were due to leakage of a single hadronic shower through the hadron calorimeter.

The hadron calorimeter was used for muon identification only for tracks which extrapolated to regions not covered by the muon chambers. In this case, muons were identified using the track segment formed from hits in the strips of the nine layers of the calorimeter. The track segment was required to have a fit quality of $\chi^2 < 5$ per degree of freedom. More than half of the layers were required to have hits, with a hit in at least one of the two outermost layers. The extrapolation of the central detector track to the hadron calorimeter was required to match the position of the calorimeter track to within 10 mrad in ϕ. Finally, the tracks were required to satisfy the same $\mathrm{d}E/\mathrm{d}x$ requirements as the muon candidates identified with the muon chambers. Use of the hadron calorimeter increased the muon identification efficiency by about 3% relative to the selection based only on the muon chambers.

2.2 Electron identification

Tracks were considered as electron candidates if the polar angle was in the range $|\cos\theta| < 0.715$, and the measured momentum was larger than 2 GeV/c.

Electrons were identified by their $\mathrm{d}E/\mathrm{d}x$, and by their energy deposition in the electromagnetic calorimeter. The identification procedure presented here has a higher efficiency and lower purity than that described in previous papers [17, 15]. The new procedure was developed to maximize the statistics in the dilepton event sample, and to eliminate selection criteria that were not well described by the detector simulation program [25]. Each electron-candidate track was first required to have a good z-coordinate measurement from the z-chambers to ensure an accurate measurement of θ. The $|\cos\theta|$ requirement ensures that the track passes through the geometrical acceptance of the z-chambers. A good θ measurement is necessary for $\mathrm{d}E/\mathrm{d}x$ measurements and for a good match between the track direction and the deposition of energy in the electromagnetic calorimeter. To ensure an accurate measurement of $\mathrm{d}E/\mathrm{d}x$, at least 40 samples were required for each track. The maximum number of samples for these tracks is 159, but samples are discarded, for example, if overlapping with those of another track.

The normalized deviation of the measured $\mathrm{d}E/\mathrm{d}x$ from that expected for an electron, $N^{\sigma}_{\mathrm{d}E/\mathrm{d}x}$, was defined by

$$N^{\sigma}_{\mathrm{d}E/\mathrm{d}x} \equiv \frac{\mathrm{d}E/\mathrm{d}x - (\mathrm{d}E/\mathrm{d}x)_0}{\sigma(\mathrm{d}E/\mathrm{d}x)}, \tag{3}$$

where $(\mathrm{d}E/\mathrm{d}x)_0$, the expected $\mathrm{d}E/\mathrm{d}x$ for an electron, and $\sigma(\mathrm{d}E/\mathrm{d}x)$, the expected measurement error, were determined using data. Electron candidates were required to satisfy $N^{\sigma}_{\mathrm{d}E/\mathrm{d}x} \geq -1.25$.

The energy associated to the track measured in the electromagnetic calorimeter is expected to be approximately equal to the measured momentum p for electrons, and to be smaller for particles other than electrons. Additional discrimination is achieved between the relatively narrow energy depositions of electrons and the depositions of hadrons by restricting the measured energy to that lying in the core of the shower, which also reduces the sensitivity to overlapping showers from nearby particles. To this end, the measured quantity E_{cone} is defined as the sum of the energy detected by those lead-glass blocks that have centres within 30 mrad of the extrapolated track position, corresponding approximately to the size of the face of a lead-glass block. The normalized deviation of the measured E_{cone}/p from that expected for an electron, $N^{\sigma}_{E_{\mathrm{cone}}/p}$, was defined by

$$N^{\sigma}_{E_{\mathrm{cone}}/p} \equiv \frac{(E_{\mathrm{cone}}/p) - (E_{\mathrm{cone}}/p)_0}{\sigma(E_{\mathrm{cone}}/p)}, \tag{4}$$

where $(E_{\mathrm{cone}}/p)_0$, the expected E_{cone}/p for an electron, and $\sigma(E_{\mathrm{cone}}/p)$, the expected measurement error, were determined using data. The distribution of $N^{\sigma}_{E_{\mathrm{cone}}/p}$ for electrons is centred at zero and has a width of about one; it is shown in Figures 1a and 1c for candidates in two momentum ranges. Electron candidates were required to satisfy $N^{\sigma}_{E_{\mathrm{cone}}/p} \geq -2$. The distributions of $N^{\sigma}_{\mathrm{d}E/\mathrm{d}x}$ for the same momentum intervals are shown in Figures 1b and 1d for candidates passing the $N^{\sigma}_{E_{\mathrm{cone}}/p}$ selection.

Electron candidates were rejected if found to be consistent with being produced through photon conversion [17].

Pairs of electron candidates were required to be separated by at least 160 mrad, otherwise the second candidate was ignored, to avoid any overlap of the energy deposited by the two candidates.

2.3 Event classification

Events were classified as single-lepton events if one and only one lepton candidate was identified in the event, and as dilepton events if at least two lepton candidates were found. The numbers of events classified in the different categories are given in Table 1.

	Single-lepton		Dilepton		Opposite jet	Same jet
	μ	24651	$\mu\mu$	1163	820	343
	e	20710	μe	1787	1241	546
			ee	882	636	246
Totals		45361		3832	2697	1135

Table 1: The numbers of single-lepton and dilepton events. The dilepton events are subdivided into opposite-jet events and same-jet events as described in Section 5.

For each event, jets were defined using the JADE algorithm [26] with the E0 recombination scheme [27]. Energy clusters in the barrel (endcap) electromagnetic calorimeter were associated to charged tracks that pointed to the cluster centroid within 150 mrad (50 mrad) in θ and 80 mrad (50 mrad) in ϕ. Both charged tracks from the central detector and energy clusters that were not associated to tracks were used in the jet-finding algorithm. The invariant mass-squared cut-off was set to $x_{\rm min} = (7\ {\rm GeV}/c^2)^2$, chosen to ensure that the jet direction provides a good estimate of the flight direction of the decaying b-flavoured hadron. The transverse momentum, $p_{\rm T}$, of each lepton candidate was calculated with respect to the axis of the jet to which it was associated by the jet-finding algorithm. This jet axis was calculated including the lepton track. The $p_{\rm T}$ distribution depends on the mass of the decaying parent hadron and so allows discrimination between leptons produced in the decay of hadrons containing b quarks, c quarks and only light quarks.

3 Monte Carlo predictions

Monte Carlo events were used to predict the distributions of prompt single leptons and dileptons as a function of the fitted parameters, where a prompt lepton is defined here to be one which originates from the decay of a b- or c-flavoured[5] hadron. The estimates of non-prompt background are described in the next section. The JETSET 7.3 Monte Carlo program [28, 29] was used to generate $\rm Z^0 \to b\bar{b}$ and $\rm Z^0 \to c\bar{c}$ events which were processed by the detector simulation package [25]. The fragmentation was parametrised using the fragmentation function of Peterson *et al.* [30] with $\epsilon_{\rm b} = 0.0035$ and $\epsilon_{\rm c} = 0.06$. This value of $\epsilon_{\rm b}$ corresponds to $\langle x_E \rangle = 0.715$. To increase the available Monte Carlo statistics, additional events which had been generated using the Lund symmetric fragmentation scheme [31] were also used. It was verified that consistent results were obtained with Peterson and Lund events. Other fragmentation functions were simulated by reweighting each Monte Carlo event according to the values of z for each b quark in the event, where z is the fragmentation parameter in the JETSET Monte Carlo [28]. For single-lepton events, only the parent b quark was taken into account in the reweighting procedure. The measurement of $\langle x_E \rangle$ presented in this paper assumes that the ratio of energies carried by the weakly-decaying hadron and the first-rank hadron is given by the JETSET Monte Carlo. The average value of this ratio is predicted to be 0.992 for b-flavoured hadrons.

The value of $\Gamma(\rm Z^0 \to c\bar{c})/\Gamma(\rm Z^0 \to hadrons)$ was taken to be 0.171 [32]. The branching ratio $B(\rm c \to \ell)$ in $\rm Z^0 \to c\bar{c}$ events was taken to be $(9.6 \pm 1.1)\%$, independent of the fitted value for $B(\rm b \to c \to \ell)$. This figure was obtained using semileptonic branching ratios for individual c-flavoured hadrons taken from the 'Review of Particle Properties' [5], assuming that their semileptonic partial widths are the same so that the semileptonic branching ratios are proportional to the lifetimes. The mix of c-flavoured hadrons produced was taken from JETSET, with uncertainties described in Reference [17]. The branching ratio $B(\rm b \to \tau \to \ell)$ was taken to be $(4.5 \pm 1.8)\%$ of $B(\rm b \to \ell)$ [17], derived from phase space arguments and the measured value of $B(\tau \to \rm e)$ [5]. The component $\rm b \to \bar{c} \to \ell$, which was kept fixed in the fits, was taken to have a branching ratio of 1.3%, the value predicted by the JETSET Monte Carlo. Decays of the

[5] The definition of prompt includes leptons from $\rm J/\psi$ decay.

type $B \to J/\psi \to \ell^+\ell^-$ were not included in these branching ratios, instead the normalisation was determined in the fit, using the $\mu^+\mu^-$ and e^+e^- mass spectra. Such J/ψ decays contribute significantly only to pairs of leptons in the same jet.

Events were reweighted to reproduce the predicted shapes of the lepton momentum distributions in the rest frame of the B or D hadron according to different decay models. Three different models were used for the $b \to \ell$ spectrum: the refined free-quark model of Altarelli *et al.* denoted ACCMM [33], the form-factor model of Isgur *et al.* denoted ISGW [34] and a modified version of this model, denoted ISGW** [20], where the normalisation of the $\bar{B} \to D^{**}\ell\nu$ component was fitted to CLEO data, and D^{**} represents a sum over the four excited D states with one unit of orbital angular momentum. The parameters of the ACCMM model were taken from a fit to CLEO data [20]. Two different models were used for the $c \to \ell$ spectrum: ACCMM and ISGW, where the parameters of the ACCMM model were fitted to DELCO data [35]. For the $b \to c \to \ell$ spectrum, the same models for $c \to \ell$ were used, but boosted by the D momentum spectrum in the B rest frame, as measured by CLEO [36]. The decays of B_s^0 and Λ_b hadrons were reweighted by the same factors as B^+ and B_d^0 decays as a function of the lepton momentum in rest frame of the decaying hadron. The masses of B_s^0 and Λ_b particles were taken to be 5.48 and 5.62 GeV/c^2 respectively.

The muon and electron identification algorithms were applied directly to the simulated events. The efficiency was found to be about 80% for muons and about 65% for electrons from b-flavoured hadron decay within the regions of geometrical acceptance.

The Monte Carlo events were generated without mixing, $\chi = 0$. To model non-zero values of χ, a fraction $2\chi(1-\chi)$ of lepton pairs from $Z^0 \to b\bar{b}$ events was changed from one charge-sign category to the other, either from opposite sign to same sign or vice versa, provided that the leptons did not originate from the same b quark.

4 Estimation of backgrounds to prompt leptons

For muon candidates, backgrounds arise from decays in flight of pions and kaons, hadrons whose interaction products penetrate the detector material (punchthrough), hadrons which do not interact strongly in the material (sailthrough) and hadrons which are incorrectly associated with muon-detector track segments (misassociation). For electron candidates, backgrounds arise from the identification of hadrons as electrons (misidentification), from photon conversions that were not rejected by the conversion finder, and from electrons produced in the decay of light hadrons (mainly Dalitz decay). Backgrounds to events containing two prompt leptons include cases where either one or both of the candidates are not prompt leptons.

4.1 Muon background

Monte Carlo $Z^0 \to$ hadrons events, generated using the JETSET program and processed through the detector simulation, were used to estimate the probability for a hadron to be

misidentified as a prompt muon, as a function of p and p_{T}. These misidentification probabilities were determined by measuring the fraction of non-prompt muon tracks that were selected by the muon identification procedure. The misidentification probability per track is about 0.6% at 5 GeV/c, about 0.4% at 10 GeV/c, and continues to decrease with increasing momentum. The accuracy of these results was studied by comparing simulation with data for the observed background in $\mathrm{K}^0 \to \pi^+\pi^-$ decays, $\tau \to 3\pi$ decays in $\mathrm{Z}^0 \to \tau^+\tau^-$ events, and samples of tracks passing some, but not all, of the muon identification requirements, as described in [17]. The tests indicated that the accuracy could be parametrised by assigning errors of 25% on the misassociation background and 50% on the punchthrough background, which predominates only at very high momenta, together with an uncertainty on the total background of 13%.

The muon background was estimated by applying these misidentification probabilities to tracks in hadronic Z^0 decays. The background to single-muon events was calculated using events without identified leptons, while the backgrounds to dilepton events were calculated using events with a single identified lepton. The fraction of tracks due to kaons is expected to be larger in single-lepton events than in an average hadronic Z^0 decay, which could lead to a change in the average muon misidentification probability. However, the effect was found to be negligible in Monte Carlo studies, largely because the misidentification probabilities for pions and kaons were similar.

This technique of muon-background estimation automatically includes cases where the muon segment is due to a decay or punchthrough, but is associated to the wrong central detector track. However, it does not include all cases where the misassociated muon segment is due to a prompt muon. This additional misassociation background was estimated using Monte Carlo $\mathrm{Z}^0 \to \mathrm{b\bar{b}}$ and $\mathrm{Z}^0 \to \mathrm{c\bar{c}}$ events, and amounted to about 0.7% of the prompt muons for tracks with momentum greater than 4 GeV/c. This background accounted for a few percent of the total muon background estimate. Approximately half of the misassociated tracks have the same charge sign as the prompt muon.

4.2 Electron background

For electrons, separate calculations were made for backgrounds from hadron misidentification, electrons from photon conversion, and electrons from the decay of light hadrons. The probability that a non-electron track is identified as an electron was estimated from the data as a function of p and p_{T}, using distributions of $N^{\sigma}_{\mathrm{d}E/\mathrm{d}x}$ and $N^{\sigma}_{E_{\mathrm{cone}}/p}$. Two distributions of $N^{\sigma}_{E_{\mathrm{cone}}/p}$ were produced:

Sample A: tracks that satisfy $N^{\sigma}_{\mathrm{d}E/\mathrm{d}x} \geq -1.25$,

Sample B: tracks that satisfy $-5 \leq N^{\sigma}_{\mathrm{d}E/\mathrm{d}x} < -3$.

Sample A consists of both electrons and non-electrons that pass the electron identification criteria except for the $N^{\sigma}_{E_{\mathrm{cone}}/p}$ requirement, while sample B consists mainly of non-electron tracks. The shape of the $N^{\sigma}_{E_{\mathrm{cone}}/p}$ distribution for non-electron tracks in sample A is represented by the shape of the distribution of sample B. In each bin of p and p_{T}, the $N^{\sigma}_{E_{\mathrm{cone}}/p}$ distribution of

sample B was scaled by a factor obtained from a likelihood fit to the region $-5 \leq N^{\sigma}_{E_{\rm cone}/p} < -3$, where almost no electrons are expected. After the scaling, the number of sample-B tracks selected by $N^{\sigma}_{E_{\rm cone}/p} \geq -2$ was taken as an estimate of the number of non-electrons among the selected tracks. The result of these fits, integrated over all bins of p and $p_{\rm T}$ is shown in Figure 2a, and split into two bins of p in Figures 1a and 1c. Shown in Figure 2b is the result of the same procedure performed on Monte Carlo events, with the contribution from known non-electrons indicated for comparison. It may be seen that the qualitative agreement between data and Monte Carlo events is good, and that the fit procedure successfully predicts the background level in the simulation. The results were checked by interchanging the use of $N^{\sigma}_{{\rm d}E/{\rm d}x}$ and $N^{\sigma}_{E_{\rm cone}/p}$ thus producing two distributions of $N^{\sigma}_{{\rm d}E/{\rm d}x}$:

Sample C: tracks that satisfy $N^{\sigma}_{E_{\rm cone}/p} \geq -2$,

Sample D: tracks that satisfy $-5 \leq N^{\sigma}_{E_{\rm cone}/p} < -3$.

Here, sample D consists mainly of non-electron tracks and was used to describe the shape of the $N^{\sigma}_{{\rm d}E/{\rm d}x}$ distribution for the non-electron tracks in sample C. In each bin of p and $p_{\rm T}$, the background in sample C was determined by fits to the $N^{\sigma}_{{\rm d}E/{\rm d}x}$ distribution, yielding results in good agreement with the fits from samples A and B. The summed results of the fits are illustrated in two bins of p in Figures 1b and 1d.

The misidentification probability for each p and $p_{\rm T}$ bin was obtained by dividing the estimated number of misidentified electrons, dominated by pions, by the total number of tracks passing the polar-angle requirement in each bin. The probability increases with increasing momentum up to a maximum of about 0.7% for momenta in the range 10 to 15 GeV/c at low $p_{\rm T}$. The probability decreases with increasing $p_{\rm T}$. The hadronic background was calculated by applying these misidentification probabilities to tracks in hadronic $\rm Z^0$ decays, as described above for the muon background calculation. The effect of a smaller pion fraction in single-lepton events was found to be small, and was taken into account.

Using information from the central detector, photon conversions were identified and rejected with an efficiency estimated to be $(84 \pm 4)\%$ for $p_{\rm T} > 0.8$ GeV/c [17] and $(79 \pm 5)\%$ for $p_{\rm T} < 0.8$ GeV/c. The respective numbers of events with one or two candidate electrons identified as conversions were used to estimate the remaining conversion background. Some candidates tagged as conversions arise from random combinations of tracks with electrons or from Dalitz decays, discussed below. The level of random combinations was assessed by seeing how many candidates were identified when the electron-candidate charge sign was flipped, i.e. looking for same-sign conversion candidates. The Monte Carlo was used to scale the wrong-sign random combinations to the expected number of right-sign random combinations. The background due to electrons from the decays of light hadrons (π^0, η, $\rm K^0_L$) was estimated using five-flavour JETSET events. About 30% of the electrons from these decays were tagged as conversions. The conversion-background estimate was corrected for this contribution.

5 Fitting procedure

In this section, the variables chosen as input to the fit and the construction of the fit are described.

Leptons from primary $b \to \ell$ decays can be separated statistically using the p and p_T of the leptons. The single-lepton events, as classified in Section 2.3, were therefore binned in p versus p_T. The yield of single-lepton events relative to the number of hadronic Z^0 decays provides information about $\Gamma_{b\bar{b}}/\Gamma_{had} \times B(b \to \ell)$ [6], and the distribution of lepton momentum at high p_T provides sensitivity to the b-quark fragmentation function. The projected p and p_T distributions are shown in Figure 3.

The opening angle between two leptons produced by two separate $b \to \ell$ decays will usually be large. Lepton-pair candidates with small opening angles may be produced by the semileptonic decays of both the b-flavoured hadron and the c-flavoured hadron in the same decay chain, by J/ψ decays or by non-prompt background. A clear separation is achieved with an opening-angle cut of 60°. Candidates with opening angle larger and smaller than 60° are henceforth referred to as opposite-jet and same-jet events, respectively.

In order to reduce the opposite-jet dilepton analysis from four dimensions to two dimensions, the variable p_{comb}, as used in our previous mixing publication [7], was constructed from p and p_T to provide good separation of the $b \to \ell$ signal from the backgrounds:

$$p_{comb} = \sqrt{\left(\frac{p}{10}\right)^2 + p_T^2}, \tag{5}$$

with p_{comb}^{min} (p_{comb}^{max}) being the smaller (larger) of the values of p_{comb} for the two leptons. In the case of events with more than two leptons, the two with the highest values of p_{comb} were chosen. The opposite-jet events were binned in p_{comb}^{min} versus p_{comb}^{max}, with p_{comb}^{min} providing the better discrimination between events with two $b \to \ell$ decays and other events, since usually at least one of the leptons comes from a $b \to \ell$ decay. The distributions of p_{comb}^{max} versus p_{comb}^{min} for different physics processes are shown in Figure 4. Sensitivity to mixing is obtained when both leptons come from the primary decay of b-flavoured hadrons, so that the charge sign of each lepton reflects the charge sign of the decaying parent b quark. Therefore, the opposite-jet dileptons were classified as opposite-sign or same-sign events according to the measured charge signs. Two distributions of events were formed: the sum of opposite-sign and same-sign events and the fraction, R, of events that are same-sign in each bin:

$$R = \frac{N(\ell^+\ell^+) + N(\ell^-\ell^-)}{N(\ell^+\ell^-) + N(\ell^+\ell^+) + N(\ell^-\ell^-)}. \tag{6}$$

The sum of the opposite-sign and same-sign events provides information about $\Gamma_{b\bar{b}}/\Gamma_{had} \times B(b \to \ell)^2$, and the fraction of events that are same-sign is sensitive to mixing. In this way, the sensitivity to mixing was kept distinct from normalisation considerations. The projected p_{comb}^{min} distributions for the sum of the events are shown in Figure 5, R versus p_{comb}^{min} is shown in Figure 6.

[6] The yield of single-lepton events is not linearly related to $\Gamma_{b\bar{b}}/\Gamma_{had} \times B(b \to \ell)$ since the relative yield of dilepton events changes with $B(b \to \ell)$, and the two samples are mutually exclusive.

For the same-jet events, the dilepton mass, m_{ll}, was chosen as a discriminating variable. This has several advantages: the J/ψ decays may be easily distinguished; the contribution from the semileptonic decay of both the b-flavoured and the c-flavoured hadrons has a reasonable separation from background; and the shape is independent of fragmentation considerations. The same-jet dileptons were also divided into opposite-sign and same-sign events. Pairs of prompt leptons essentially contribute only to the opposite-sign category, which provides information on $\Gamma_{\mathrm{b\bar{b}}}/\Gamma_{\mathrm{had}} \times B(\mathrm{b} \to \ell) \times B(\mathrm{b} \to \mathrm{c} \to \ell)$, from which $B(\mathrm{b} \to \mathrm{c} \to \ell)$ is obtained. (It is difficult to study $\mathrm{b} \to \mathrm{c} \to \ell$ decays in the single-lepton channel because of high background at low p_{T}. There is sensitivity to $\mathrm{b} \to \mathrm{c} \to \ell$ decays in the opposite-jet dileptons, but the signal is much less clean than in the same-jet events.) The same-sign events are dominated by background and provide a test of the background calculations. The distributions of m_{ll} are shown in Figure 7.

The results were extracted using a binned maximum likelihood technique. The total likelihood, $\mathcal{L}$, was the product,

$$\mathcal{L} = \mathcal{L}_{\mathrm{single}} \times \mathcal{L}_{\mathrm{oppjet}} \times \mathcal{L}_{\mathrm{R}} \times \mathcal{L}_{\mathrm{samejet}}, \tag{7}$$

where $\mathcal{L}_{\mathrm{single}}$ represents the likelihood for the single-lepton events, $\mathcal{L}_{\mathrm{oppjet}}$ for the opposite-jet dilepton events (sum of opposite-sign and same-sign events), $\mathcal{L}_{\mathrm{R}}$ for the same-sign event fraction in the opposite-jet events, and $\mathcal{L}_{\mathrm{samejet}}$ for the opposite-sign same-jet events. The same-sign same-jet events were not included in the fit, since they contain essentially no signal. For the single lepton events, muons and electrons were kept separated, and the dilepton events were split up into $\mu\mu$, μe and ee events. The likelihood of the data was calculated from the observed and predicted quantities, whether numbers of events or ratios, in each bin. The predictions were summed over contributions from the Monte Carlo and background calculations, where the different Monte Carlo contributions were adjusted according to the parameters in the fit and to the number of hadronic events selected in the data before any lepton requirements. The backgrounds to prompt leptons were kept fixed in the fit. Poisson statistics were used for the dilepton event distributions, so that

$$\mathcal{L}_{\mathrm{oppjet}} = \prod_{p_{\mathrm{comb}}^{\mathrm{min}}, p_{\mathrm{comb}}^{\mathrm{max}}} \frac{\mu^n \mathrm{e}^{-\mu}}{n!} \tag{8}$$

and

$$\mathcal{L}_{\mathrm{samejet}} = \prod_{m_{ll}} \frac{\mu^n \mathrm{e}^{-\mu}}{n!}, \tag{9}$$

where the products are over bins in $p_{\mathrm{comb}}^{\mathrm{min}}$ and $p_{\mathrm{comb}}^{\mathrm{max}}$ for the opposite-jet dileptons and m_{ll} for the same-jet dileptons. In each case, n represents the number of events observed in a given bin and μ represents the predicted number of events. The binomial distribution was assumed for the same-sign event fraction:

$$\mathcal{L}_{\mathrm{R}} = \prod_{p_{\mathrm{comb}}^{\mathrm{min}}, p_{\mathrm{comb}}^{\mathrm{max}}} \frac{n!}{m!(n-m)!} R^m (1-R)^{n-m}, \tag{10}$$

where the product is over bins in $p_{\mathrm{comb}}^{\mathrm{min}}$ and $p_{\mathrm{comb}}^{\mathrm{max}}$, m is the number of like-sign events in a given bin, and R is the predicted fraction of events that are like-sign. For the single leptons, where the statistics in each bin were relatively high, the likelihood functions were taken to be Gaussian in each bin:

$$\mathcal{L}_{\mathrm{single}} = \prod_{p, p_{\mathrm{T}}} \exp\left(-\frac{(n-\mu)^2}{2(\mu + \sigma_\mu^2)} \right), \tag{11}$$

where the product was over bins in p and $p_{\rm T}$, and σ_μ indicates the statistical error on μ. The widths of these Gaussians took account of the statistical errors both on the data and on the prediction, essential to avoid bias on the fragmentation measurement due to statistical error incurred in the procedure of reweighting Monte Carlo events. The effect of limited statistical precision for the predicted dilepton distributions is included in the systematic errors. The fragmentation parameter used in the fit was $\langle x_E \rangle$ for b-flavoured hadrons. The predicted distributions for the single-lepton and dilepton events were generated for seven values of $\langle x_E \rangle$ by the reweighting procedure mentioned in Section 3, covering the range from 0.679 to 0.737. Other values of $\langle x_E \rangle$ were constructed in the fit by linear interpolation between the nearest generated values on each side.

The fit weights bins appropriately to take into account the degradation in statistical sensitivity due to background contamination. However, it does not take into account systematic uncertainties on the background. It is therefore important to exclude regions from the fit which have large background systematic uncertainties. The single-lepton sample has relatively high statistics, so stringent requirements may be placed against backgrounds. The single-lepton criteria were chosen so that the non-prompt background accounted for no more than 10% of the data in any bin, which also reduced the contribution from $\mathrm{c} \to \ell$ and $\mathrm{b} \to \mathrm{c} \to \ell$ decays to a low level, while selecting a sufficient number of $\mathrm{b} \to \ell$ decays. Single muons were required to satisfy $p > 5\,\mathrm{GeV}/c$ and $p_{\rm T} > 1.4\,\mathrm{GeV}/c$ or $p > 7\,\mathrm{GeV}/c$ and $p_{\rm T} > 1.2\,\mathrm{GeV}/c$. Single electrons were required to satisfy $p > 2\,\mathrm{GeV}/c$ and $p_{\rm T} > 1.2\,\mathrm{GeV}/c$. The opposite-jet dilepton requirements were designed to select mainly events that have two $\mathrm{b} \to \ell$ decays. Although a significant fraction of these events were rejected by the requirements, only small improvements in statistical precision could be made by relaxing them. The selection criteria were $p^{\rm min}_{\rm comb} > 1.4\,\mathrm{GeV}/c$ for $\mu\mu$ events, $p^{\rm min}_{\rm comb} > 1.3\,\mathrm{GeV}/c$ for μe events and $p^{\rm min}_{\rm comb} > 1.2\,\mathrm{GeV}/c$ for ee events. The reason for the difference in these criteria is that the electrons have a softer spectrum due to bremsstrahlung and the lower momentum requirement, and that the identification efficiency is lower for electrons from $\mathrm{b} \to \mathrm{c} \to \mathrm{e}$ decays than for electrons from $\mathrm{b} \to \mathrm{e}$ decays. In the likelihood calculation, this selection was applied only to the distributions of the sum of opposite-sign and same-sign opposite-jet events. Looser requirements were applied to the distributions of the same-sign event fraction R (containing the mixing signal): $p^{\rm min}_{\rm comb} > 1.2\,\mathrm{GeV}/c$, $1.1\,\mathrm{GeV}/c$ and $1.0\,\mathrm{GeV}/c$ for $\mu\mu$, μe and ee events respectively. This was done because the fitted value of χ is much less sensitive to non-prompt background systematic uncertainties than are the fitted values of the branching ratios. The opposite-sign same-jet events were required to satisfy $m_{ll} > 1.5$ GeV/c^2 for $\mu\mu$ events, $m_{ll} > 1.2$ GeV/c^2 for μe events and $m_{ll} > 1.0$ GeV/c^2 for ee events, mass regions relatively free from backgrounds.

The result of the fit, using the ACCMM decay models for both $\mathrm{b} \to \ell$ and $\mathrm{c} \to \ell$ decays, is given in Table 2. The errors in the table are statistical only. The distributions predicted using these fitted values are shown as the solid histograms in Figures 3, 5, 6 and 7. The fitted value for $B(\mathrm{b} \to \mathrm{J}/\psi)$, which assumes $B(\mathrm{J}/\psi \to \ell^+\ell^-) = 6.15\%$ [5], is compatible with the world average [5]. This parameter was allowed to vary to avoid introducing bias on the measurement of $B(\mathrm{b} \to \mathrm{c} \to \ell)$, but it is not intended as a measurement. Also given in Table 2 are the results using the ISGW and ISGW** models for the $\mathrm{b} \to \ell$ decays (ACCMM for $\mathrm{c} \to \ell$ decays). The matrix of correlation coefficients obtained from the fit is given in Table 3. To indicate the quality of the fit, a chi-squared was calculated (not minimised) to be 152.7 for 138 degrees of freedom.

	ACCMM	ISGW	ISGW**
χ	$0.143^{+0.022}_{-0.021}$	$0.141^{+0.022}_{-0.021}$	$0.144^{+0.022}_{-0.020}$
$\Gamma_{b\bar{b}}/\Gamma_{had}$	0.222 ± 0.011	0.219 ± 0.011	0.226 ± 0.011
$B(b \to \ell)$	$(10.5 \pm 0.6)\%$	$(10.3 \pm 0.6)\%$	$(11.0 \pm 0.6)\%$
$B(b \to c \to \ell)$	$(7.7 \pm 0.4)\%$	$(7.9 \pm 0.4)\%$	$(7.5 \pm 0.4)\%$
$B(b \to J/\psi)$	$(0.92^{+0.16}_{-0.15})\%$	$(0.92^{+0.16}_{-0.15})\%$	$(0.93^{+0.16}_{-0.15})\%$
$\langle x_E \rangle$	0.697 ± 0.006	0.694 ± 0.006	0.700 ± 0.006

Table 2: Fit results for different $b \to \ell$ decay models. The central result uses the ACCMM model.

	χ	$\Gamma_{b\bar{b}}/\Gamma_{had}$	$B(b \to \ell)$	$B(b \to c \to \ell)$	$B(b \to J/\psi)$	$\langle x_E \rangle$
χ	1.	-0.12	$+0.14$	-0.14	0.00	-0.05
$\Gamma_{b\bar{b}}/\Gamma_{had}$		1.	-0.92	$+0.08$	-0.23	$+0.02$
$B(b \to \ell)$			1.	-0.15	$+0.19$	-0.14
$B(b \to c \to \ell)$				1.	-0.07	-0.04
$B(b \to J/\psi)$					1.	-0.08
$\langle x_E \rangle$						1.

Table 3: The correlation coefficients for the parameters in the fit using the ACCMM model.

6 Cross checks

The above results were found to be stable when the single-lepton p_T requirements were changed by ± 0.2 GeV/c, and when the dilepton p^{min}_{comb} and m_{ll} requirements were changed by ± 0.2 GeV/c and ± 0.2 GeV/c^2. No significant changes were observed when the single-muon requirements were simplified to $p > 5$ GeV/c and $p_T > 1.2$ GeV/c. The influence of single-lepton bins containing less than 50 events was found to be small. Such bins could conceivably bias the result, since Gaussian errors were assumed for the single-lepton distributions.

In order to cross check the results, a much simpler fit was constructed. The binning of the distributions input to the fit was changed so that all the data selected from each distribution was represented by only one bin per distribution, with the same kinematic requirements as above. Such a fit is sensitive neither to $\langle x_E \rangle$ nor to $B(b \to J/\psi)$, so these parameters were fixed to 0.70 and 0.9% respectively. The results of this fit, using the ACCMM model for $b \to \ell$ and $c \to \ell$ decays, were

$$\begin{aligned} \chi &= 0.132^{+0.024}_{-0.023} \\ \Gamma_{b\bar{b}}/\Gamma_{had} &= 0.225^{+0.012}_{-0.011} \\ B(b \to \ell) &= (10.3 \pm 0.6)\% \\ B(b \to c \to \ell) &= (7.9 \pm 0.4)\%. \end{aligned}$$

These results are consistent with those quoted in the previous section. The numbers of events

used in this fit together with the predicted numbers and purities after the fit are given in Table 4. In this context purity is defined as the fraction of events from b $\to \ell$ decays for the single leptons and the fraction with two b $\to \ell$ decays for the opposite-jet dilepton events. In the same-jet dilepton events, the purity refers to the fraction containing both b $\to \ell$ and b $\to$ c $\to \ell$ decays.

	Number observed	Number predicted	Purity
Single μ	4248	4206	0.82
Single e	2719	2767	0.80
Total	6967	6973	0.82
Opposite jet $\mu\mu$	160	164	0.76
Opposite jet μe	229	225	0.70
Opposite jet ee	98	97	0.73
Total	487	486	0.73
Same jet $\mu\mu$	166	158	0.67
Same jet μe	257	268	0.82
Same jet ee	169	164	0.70
Total	592	590	0.75

Opposite-jet events for same-sign fraction			
	Number of events	R	Predicted R
$\mu\mu$	269	0.34 ± 0.03	0.32
μe	358	0.30 ± 0.02	0.34
ee	159	0.40 ± 0.04	0.34
Total	786	0.332 ± 0.017	0.334

Table 4: The numbers of events selected by the p, $p_{\rm T}$, $p_{\rm comb}^{\rm min}$ and m_{ll} requirements. Also given are the fractions, R, of opposite-jet events where both leptons have the same charge-sign. The predicted numbers and purities are taken from the simple fit to these events.

In order to cross check the fragmentation result, $\langle x_E \rangle$ was estimated from the mean lepton momentum in the single-lepton events. The simple fit described above was repeated for $\langle x_E \rangle = 0.68$ and 0.72, and the resulting mean lepton momentum calculated for the single-lepton events passing the kinematic cuts. These values are compared to the data in Table 5. The mean

	Data	$\langle x_E \rangle = 0.68$	$\langle x_E \rangle = 0.70$	$\langle x_E \rangle = 0.72$
Mean p for μ	12.05 ± 0.08	11.87	12.07	12.28
Mean p for e	10.41 ± 0.11	10.09	10.32	10.53

Table 5: The mean lepton momentum in single lepton events, compared to predictions for different values of $\langle x_E \rangle$.

lepton momenta give values of $\langle x_E \rangle = 0.698 \pm 0.008$ for the muons, and $\langle x_E \rangle = 0.708 \pm 0.010$

for the electrons. The weighted average, $\langle x_E \rangle = 0.701 \pm 0.006$, is consistent with the previous value. Note that, in this case, the statistical error does not include any contribution from Monte Carlo statistics.

A further cross check was to repeat the fit performed in the previous section, using muons and electrons by themselves. For the fit with muons, electron candidates were ignored and vice versa. Thus events with both a muon and an electron candidate entered in both the single-muon and single-electron categories for these fits. The results are shown in Table 6. The muon and

	muon only	electron only
χ	0.16 ± 0.04	$0.24^{+0.09}_{-0.06}$
$\Gamma_{\mathrm{b\bar{b}}}/\Gamma_{\mathrm{had}}$	$0.235^{+0.021}_{-0.019}$	$0.211^{+0.027}_{-0.023}$
$B(\mathrm{b} \to \ell)$	$(10.1^{+1.0}_{-0.9})\%$	$(10.9^{+1.4}_{-1.3})\%$
$B(\mathrm{b} \to \mathrm{c} \to \ell)$	$(8.3 \pm 0.8)\%$	$(8.9^{+0.9}_{-0.8})\%$
$B(\mathrm{b} \to \mathrm{J}/\psi)$	$(0.7 \pm 0.2)\%$	$(1.2 \pm 0.3)\%$
$\langle x_E \rangle$	0.699 ± 0.008	0.701 ± 0.009

Table 6: Results from fits to muons and electrons separately.

electron results agree with each other and with the result of the full fit given in the previous section.

7 Systematic errors

The systematic errors were estimated by changing each assumption in turn by its uncertainty, and repeating the fit. When errors were determined to be asymmetric, the r.m.s. of the positive and negative components was taken. The errors are summarised in Table 7, and the correlation coefficients for the full errors, including both statistical and systematic contributions, are given in Table 8. Where possible, the signs of the errors ($\pm$ or $\mp$) indicate the relative direction of change for each parameter.

7.1 Modelling and branching-ratio uncertainties

The error from the $\mathrm{b} \to \ell$ decay modelling was taken directly from Table 2. The error from the $\mathrm{c} \to \ell$ decay model, which affects both the $\mathrm{b} \to \mathrm{c} \to \ell$ decays and the $\mathrm{c} \to \ell$ decays in $\mathrm{Z}^0 \to \mathrm{c\bar{c}}$ events, was estimated by using the ISGW model for this decay. The error coming from $B(\mathrm{c} \to \ell)$ in $\mathrm{Z}^0 \to \mathrm{c\bar{c}}$ events was assessed by varying it in the range $(9.6 \pm 1.1)\%$, as described in Reference [17]. An uncertainty of 22% was allowed on the value of $\Gamma(\mathrm{Z}^0 \to \mathrm{c\bar{c}})/\Gamma(\mathrm{Z}^0 \to \mathrm{hadrons})$, corresponding to the precision of the OPAL measurement based on D^* tagging [37]. A range of $\pm 0.5\%$ about the central value of 1.3% was allowed for $B(\mathrm{b} \to \bar{\mathrm{c}} \to \ell)$, which allows for a $\bar{\mathrm{c}}$ quark to be produced in $(15 \pm 5)\%$ of b quark decays, with a relative uncertainty of 15% on the semileptonic branching ratio of the mix of c-flavoured hadrons produced. The value of

$B(\mathrm{b} \to \tau \to \ell)$ was varied between 2.7% and 6.3% of $B(\mathrm{b} \to \ell)$, a range which was mentioned above. The fragmentation-model error was assessed by using different parametrisations for the distribution of z in the reweighting procedure. The parametrisations considered were: Lund, Collins-Spiller, Kartvelishvili, and Bowler-Morris [31,38]. The errors were calculated by taking the r.m.s. deviation of each parameter from the results obtained using the Peterson function. The uncertainty due to charm fragmentation was assessed by using $\langle x_E \rangle_{\mathrm{c}} = 0.51 \pm 0.02$. The Monte Carlo events were generated without any polarisation of b-flavoured baryons. The effect of including a 94% polarisation, the full polarisation of the b quark, was estimated using the results of Mannel and Schuler [39], and is included in Table 7.

	χ	$\Gamma_{\mathrm{b\bar{b}}}/\Gamma_{\mathrm{had}}$	$B(\mathrm{b} \to \ell)$	$B(\mathrm{b} \to \mathrm{c} \to \ell)$	$\langle x_E \rangle$
$\mathrm{b} \to \ell$ decay model	± 0.002	± 0.003	$\pm 0.32\%$	$\mp 0.21\%$	± 0.003
$\mathrm{c} \to \ell$ decay model	± 0.001	± 0.001	$\pm 0.05\%$	$\pm 0.34\%$	0.
$B(\mathrm{c} \to \ell)$	± 0.002	∓ 0.001	$\mp 0.01\%$	$\pm 0.04\%$	0.
$\Gamma(\mathrm{Z}^0 \to \mathrm{c\bar{c}})/\Gamma(\mathrm{Z}^0 \to \mathrm{hadrons})$	± 0.003	∓ 0.003	$\pm 0.05\%$	$\pm 0.07\%$	0.
$B(\mathrm{b} \to \bar{\mathrm{c}} \to \ell)$	0.	± 0.001	$\mp 0.06\%$	$\mp 0.07\%$	0.
$B(\mathrm{b} \to \tau \to \ell)$	0.	± 0.001	$\mp 0.07\%$	$\mp 0.04\%$	0.
b fragmentation model	± 0.001	∓ 0.001	$\mp 0.16\%$	$\mp 0.07\%$	± 0.009
Charm fragmentation	± 0.001	∓ 0.002	$\pm 0.04\%$	$\pm 0.05\%$	∓ 0.001
b baryon polarisation	0.	0.	-0.01%	$+0.08\%$	-0.004
$\mathrm{b} \to \mathrm{c} \to \ell$ problem:					
a) D momentum spectrum	± 0.003	∓ 0.001	$\pm 0.06\%$	$\mp 0.37\%$	0.
b) BR difference	± 0.003	∓ 0.001	$\pm 0.04\%$	$\mp 0.32\%$	0.
μ identification efficiency	± 0.001	± 0.001	$\pm 0.24\%$	$\pm 0.13\%$	± 0.001
μ polar angle measurement	0.	± 0.001	$\mp 0.02\%$	$\mp 0.01\%$	0.
e identification efficiency	± 0.001	∓ 0.001	$\pm 0.18\%$	$\pm 0.14\%$	∓ 0.001
e bremsstrahlung	0.	0.	$\pm 0.04\%$	$\pm 0.01\%$	0.
μ background	± 0.001	∓ 0.002	$\pm 0.09\%$	$\mp 0.06\%$	∓ 0.002
e misidentification background	0.	± 0.001	$\mp 0.02\%$	$\pm 0.03\%$	± 0.001
e conversion background	0.	± 0.001	$\mp 0.02\%$	$\mp 0.09\%$	0.
e decay background	± 0.001	0.	$\pm 0.01\%$	$\mp 0.08\%$	0.
Monte Carlo statistics	0.003	0.003	0.22%	0.14%	0.001
TOTAL	0.007	0.007	0.55%	0.71%	0.011

Table 7: Systematic errors. The sign of the error for each parameter relative to those for the other parameters is indicated by $\pm$ or $\mp$.

A more involved error comes from the way that the $\mathrm{b} \to \mathrm{c} \to \ell$ component is fitted, referred to the $\mathrm{b} \to \mathrm{c} \to \ell$ problem in Table 7. Since the contribution of $\mathrm{b} \to \mathrm{c} \to \ell$ decays to the opposite-jet region is suppressed by the $p^{\mathrm{min}}_{\mathrm{comb}}$ requirements, the fit is sensitive mainly to the same-jet region, where the c-flavoured hadrons are produced in semileptonic decays of b-flavoured hadrons. However, the result for $B(\mathrm{b} \to \mathrm{c} \to \ell)$ quoted above is intended as a measurement of the average branching ratio for the semileptonic decay of c-flavoured

	χ	$\Gamma_{b\bar{b}}/\Gamma_{had}$	$B(b \to \ell)$	$B(b \to c \to \ell)$	$\langle x_E \rangle$
χ	1.	-0.15	$+0.18$	-0.16	$+0.02$
$\Gamma_{b\bar{b}}/\Gamma_{had}$		1.	-0.52	$+0.04$	$+0.08$
$B(b \to \ell)$			1.	-0.07	-0.11
$B(b \to c \to \ell)$				1.	-0.16
$\langle x_E \rangle$					1.

Table 8: The full correlation coefficients, including both statistical and systematic errors.

hadrons produced in inclusive decays of b-flavoured hadrons. The mix of c-flavoured hadrons produced in such decays may be different from that resulting from the semileptonic decays of b-flavoured hadrons, and these c-flavoured hadrons may have a different momentum spectrum. The sensitivity of the measured $B(b \to c \to \ell)$ to such differences is discussed in the following paragraphs. In these paragraphs, B meson signifies a B^0_d or B^+ meson, and the systematic errors for B^0_s and b-baryon decays are assumed to be completely correlated with those for B meson decays. This assumption leads to larger overall errors compared to assigning significantly larger, but uncorrelated, errors for the B^0_s and b-baryon decays.

The effect of possible differences in the momentum spectra are considered first. Direct measurements of the momentum spectra of D mesons produced in inclusive decays of B mesons have been made by CLEO [36]. No such measurements are available for D mesons produced in semileptonic B decays. Instead, the momentum spectra for such D mesons were taken from a toy Monte Carlo based on the ISGW model of semileptonic B decays. The relative production rates of D, D^* and D^{**} in the model were adjusted to the CLEO and ARGUS measurements [40], so that D^{**} mesons were produced in 35% of the decays. The model assumes that all the semileptonic decays are three-body decays. The subsequent decays of the D^* and D^{**} mesons to D mesons are not described by the model, but must be simulated to calculate the D momentum spectrum in the B rest frame. The D^{**} mesons were assumed to decay to $D^*\pi$ 50% of the time and to $D\pi$ 50% of the time, but the conclusions were not sensitive to the relative rates. The D^* mesons produced in these decays were assumed to decay to $D\pi$ or $D\gamma$ according to the measured branching ratios [5]. The predicted D momentum spectrum (in the B rest frame) from semileptonic B decay had a mean larger by about 15% than that measured for inclusive B decays. This translates into a difference of only 5% in the mean D energy, since the D mass is large compared to the mean D momentum in the B rest frame. The difference in the momentum spectra was used to reweight the same-jet $b \to c \to \ell$ decays to estimate the systematic error labelled a) in Table 7. This is reasonably conservative, since a significant four-body component in the semileptonic case could improve the agreement.

The mix of c-flavoured hadrons produced in semileptonic decays may differ from that produced in inclusive decays of b-flavoured hadrons. Because of the large differences in the semileptonic branching ratios of different c-flavoured hadrons, this would lead to a different value for the average branching fraction of $b \to c \to \ell$ in the two cases. In particular, CLEO [36] has measured the inclusive branching ratio $B(B \to \Lambda_c X) = (6.4 \pm 1.1)\%$. Because of the large rest mass of the Λ_c and the associated antibaryon that would have to be produced, it is reasonable to assume that the production rate of Λ_c baryons is negligible in semileptonic B meson decays

(but not in Λ_b decays). The central value of the fit was corrected for this effect, assuming that the semileptonic branching ratio for the Λ_c is 3.2%, calculated from the measured lifetime [5]. Other possible differences between the same-jet and opposite-jet $b \to c \to \ell$ branching ratios were assumed to be accounted for by a possible difference in the rate of D^0 production relative to D^+ production between the semileptonic and inclusive B decays. Direct decays of B mesons to D^0 and D^+ are assumed to occur at the same rate. However, differences in the total D^0 and D^+ rates will occur due to the production of D^{*0} and D^{*+}. An equal mix of these D^* states could be expected to decay to D^0 with a total branching ratio of $(77.5 \pm 2)\%$ [5]. The possible difference between inclusive and semileptonic decays was therefore assessed by considering the relative branching ratio of B to D^* in the two cases. Inclusive measurements of $B(B \to D^{*\pm}X)$ from CLEO and ARGUS, averaged in Reference [5], can be used to infer $B(B \to D^*X) = 0.54 \pm 0.07$, assuming that the branching ratio of B to $D^{*0}X$ is the same as that to $D^{*+}X$. The branching fraction of B mesons to D^* as a fraction of the non-Λ_c decays is

$$f^*_{\rm incl} = 0.58 \pm 0.08. \tag{12}$$

This is the relevant quantity for inclusive decays, since a separate correction is made for decays to Λ_c particles. For the semileptonic decays, ARGUS [41] has recently measured the production of $D^{*\pm}$ from D^{**} decays in semileptonic B decays (the measurement in principle includes non-resonant $D^{*\pm}$ production). From their measurements can be deduced

$$B(B \to D^{**}\ell\nu) \times B(D^{**} \to D^*X) = 0.021 \pm 0.004 \pm 0.004, \tag{13}$$

if one assumes that the B^+ and B^0 branching ratios are the same, and that the D^{*0} production rate is the same as that for the D^{*+}. For the total D^* production rate, this indirect branching fraction must be added to the branching ratio for direct $B \to D^*\ell\nu$ decays. For the latter branching ratio, the recent measurement in Reference [41] is averaged with the previous world average [5] yielding 0.50 ± 0.06. The fraction of D^* produced in semileptonic decay is given by

$$f^*_\ell = \frac{B(B \to D^{**}\ell\nu) \times B(D^{**} \to D^*X) + B(B \to D^*\ell\nu)}{B(B \to \ell\nu X)}, \tag{14}$$

where the denominator is the semileptonic branching ratio of the B, which is taken to be 0.108 ± 0.006 [20]. Thus, $f^*_\ell = 0.66 \pm 0.08$, compatible with being equal to the value of $f^*_{\rm incl}$. The difference is 0.08 ± 0.11. The error on this difference translates to a systematic error of 0.29% (a relative error of 3.6%) on the difference between the same-jet and opposite-jet $b \to c \to \ell$ branching ratios. However, some of the assumptions made above would be incorrect if the B^0_d and B^+ lifetimes differ by 10%. This effect was taken into account by assuming that the semileptonic branching ratios scale with the lifetime, and that the difference in lifetimes is accounted for by a difference in $\Gamma(B \to D^{\pm}X)$ for B^0_d and B^+ mesons. The latter assumption is a conservative one, since D^+ mesons are produced in a much smaller fraction of B decays than are D^0 mesons. The total systematic error on the difference between the same-jet and opposite-jet $b \to c \to \ell$ branching ratios is 0.4% (a relative error of 5%), and the effect is labelled b) in Table 7. The errors on the branching fraction to Λ_c and the Λ_c semileptonic branching ratio are negligible by comparison. Direct measurements of the D^+ and D^0 production rates [5] in semileptonic and inclusive B decays are consistent.

In addition to these errors, another effect was considered. The b-flavoured hadrons in $b \to c \to \ell$ decays were assumed to undergo the same rate of mixing as for those in $b \to \ell$

decays. However, this may not be true, since the semileptonic branching ratios of different D mesons differ appreciably, allowing B^+, B_d^0 and B_s^0 to contribute with different weights to the $b \to c \to \ell$ component. The effect was estimated using the JETSET Monte Carlo values for these branching ratios, resulting in a change in χ of only 0.0002. The effect was neglected.

7.2 Lepton identification efficiencies and backgrounds

Comparisons of the muon identification efficiencies for events from $Z^0 \to \mu^+\mu^-$ and from the two-photon process $e^+e^- \to e^+e^-\mu^+\mu^-$ with those from Monte Carlo simulations showed good agreement. These comparisons were described in Reference [17], where the polar-angle range was limited to $|\cos\theta| < 0.9$, and muons identified using the hadron calorimeter were not included. The identification efficiencies in the region $0.9 < |\cos\theta| < 0.95$ and in the selection of muons with the hadron calorimeter were checked by comparing the rates of muons selected in these regions relative to the total rate of muons selected in hadronic events. The Monte Carlo simulation was in good agreement with the data as a function of p and p_T in each case. The uncertainty on the efficiency of the dE/dx requirement in hadronic events was assessed using low-momentum pions and pions from $K^0 \to \pi^+\pi^-$ decays. The overall uncertainty on the muon efficiency was estimated to be 4.2%. The uncertainty on the shape of the efficiency with respect to p_T was parametrised by reducing the efficiency coherently by 3% for $p_T < 0.5\,\mathrm{GeV}/c$ and by 1.5% for $0.5\,\mathrm{GeV}/c < p_T < 1.0\,\mathrm{GeV}/c$, while keeping the efficiency fixed for $p_T > 1.0\,\mathrm{GeV}/c$. The overall normalisation change gave the larger variations. Since z-chamber hits are not required for muon candidates, some of these candidates will have an error on the θ measurement which significantly affects the measured p_T. The systematic error assigned allows for inaccuracy in the simulation of this effect.

The uncertainty in the electron identification efficiency was determined separately for each of the selection criteria described in Section 2.2. The errors in the simulation of the efficiencies of the polar angle cut, the z-coordinate requirement and the cut on the number of dE/dx samples were estimated as a function of p, p_T and $\cos\theta$ using muons identified without any dE/dx requirements. For large p_T, these errors range from 1.4% at normal incidence to 8.3% at large angles. The uncertainty in the simulation of the $N^{\sigma}_{dE/dx}$ efficiency was determined to be 2.0% from a comparison between data and Monte Carlo for electrons in hadronic events. By varying the modelling of E_{cone} within a range allowed by electrons from single-track events, the uncertainty in the $N^{\sigma}_{E_{\mathrm{cone}}/p}$ efficiency was estimated to be 1.2%. These events are produced mainly by two-photon processes and radiative bhabha scattering. The efficiency was checked for electrons in hadronic events and for identified photon conversions. Good agreement was observed between Monte Carlo and data in both cases. In addition, uncertainties in the efficiency due to the track environment of each source of prompt electrons were determined using the Monte Carlo. Inaccuracy in the simulation of the amount of material between the interaction point and the end of the jet chamber causes an error in the predicted amount of electron bremsstrahlung, and hence in the prediction for the reconstructed electron momentum distribution.

The error from the muon-background estimate [17] has three components, corresponding to the uncertainties described in Section 4.1. The punchthrough background was varied by

50%. The misassociation background was varied by 25%, which affects mainly background at low p_{T}, and thus has a very small effect on the results of the fit since this region is largely excluded. The overall normalisation of the background was changed by 13%. The systematic error on the electron misidentification background has two components. The calculation of the misidentification probabilities was repeated using Monte Carlo events, giving probabilities different by typically 20% from those obtained from the data. Large differences here would indicate that the Monte Carlo events could not be used to provide an accurate check of the background-calculation procedure. To cover this possibility, results were obtained using these different misidentification probabilities, and half of the difference between these results and the central values was assigned as systematic error. The difference between these calculated Monte Carlo probabilities and the probabilities obtained from known Monte Carlo non-electrons was assigned as an additional systematic uncertainty, as an estimate of the error introduced by the method of calculating the misidentification probabilities. The uncertainty on the background to electrons from photon conversions was assessed by varying the total estimated background by 30%, corresponding to the uncertainty on the tagging efficiency of $(84 \pm 4)\%$ for $p_{\mathrm{T}} > 0.8\,\mathrm{GeV}/c$ and $(79 \pm 5)\%$ for $p_{\mathrm{T}} < 0.8$ GeV/c. The error due to the p_{T} dependence of this efficiency was calculated by comparing results obtained assuming an efficiency independent of p_{T}. The uncertainty due to light-hadron decay to electrons was estimated conservatively by varying this source of background by 50%.

7.3 Monte Carlo statistics

The effect of the limited Monte Carlo statistics for the single-lepton distributions is included in the statistical errors quoted for the fit. The errors due to the Monte Carlo statistics of the dilepton distributions were assessed by repeating the fit using the method of least squares rather than maximum likelihood, with the Monte Carlo statistical error included. The results from this fit were then compared with those from another least-squares fit, which did not have the Monte Carlo statistical error included for the dileptons (both fits included the statistical error in the single leptons, since this is also included in the likelihood fit). The systematic errors were taken to be the difference in quadrature between the errors of these two fits. This procedure is valid if the statistical error due to Monte Carlo statistics in the least-squares fit is similar to that in the likelihood fit. The statistical errors due to the data were found to be similar in the two fits, indicating that the above assumption is reasonable.

8 Discussion and conclusion

Combining the OPAL measurement of χ with the value $\chi_{\mathrm{d}} = 0.149 \pm 0.023 \pm 0.019 \pm 0.010$ measured by CLEO [4], information can be obtained on χ_{s}, the mixing parameter for the $\mathrm{B_s^0}$. The result depends critically on f_{s}, which, while it has not been accurately measured, is estimated to be about 12% [42]. Assuming that equal fractions of $\mathrm{B_d^0}$ and $\mathrm{B^+}$ mesons are produced, and that the fraction of b-flavoured baryons is $(9.0 \pm 4.5)\%$, constraints can be placed on the relation between χ_{s} and f_{s}. This constraint is not very sensitive to the assumed baryon fraction, and a 50% uncertainty on this fraction is included. The result is shown in

Figure 8 together with the one-standard-deviation errors. The data are consistent with full B_s^0 mixing ($\chi_s = 0.5$) when f_s is near the predicted value of 0.12. If one assumes $\chi_s = 0.5$, then the data imply $f_s = 0.18 \pm 0.06$. Our measured value for χ is consistent with previous measurements [6–8].

The measured value of $\Gamma_{b\bar{b}}/\Gamma_{had}$ combined with the OPAL measurement of the Z^0 hadronic width, $\Gamma_{had} = (1738 \pm 12)$ MeV [10], gives a measurement of $\Gamma_{b\bar{b}} = (386 \pm 23)$ MeV, in good agreement with a standard-model prediction of (376 ± 2) MeV [32] and previous measurements [11–18]. The measurement presented in Reference [17] is based on the same data, and has a similar overall error. That measurement was deduced from the yield of leptons at high values of p_T together with semileptonic branching ratios measured by CLEO [20], giving rise to errors largely independent from those quoted above. The measurement presented in Reference [18] is based on a subset of the same data, and has a slightly smaller overall error. The errors are almost completely independent, since that measurement uses an impact parameter technique which makes no use of lepton identification. The fit was repeated with the value of $\Gamma_{b\bar{b}}/\Gamma_{had}$ fixed to 0.217, in agreement with standard-model predictions, giving

$$\begin{aligned} \chi &= 0.145^{+0.021}_{-0.020} \pm 0.007 \\ B(b \to \ell) &= (10.8 \pm 0.2 \pm 0.6)\% \\ B(b \to c \to \ell) &= (7.7 \pm 0.4 \pm 0.7)\% \\ \langle x_E \rangle &= 0.696 \pm 0.006 \pm 0.010, \end{aligned}$$

where no systematic error due to uncertainty on $\Gamma(Z^0 \to c\bar{c})/\Gamma(Z^0 \to \text{hadrons})$ was included. Only the value of $B(b \to \ell)$ is significantly different from that quoted for the main result, as should be expected from the correlation coefficients shown in Table 3.

The result for $B(b \to \ell)$ is the first such measurement from OPAL which does not assume a value for $\Gamma_{b\bar{b}}/\Gamma_{had}$. It is in good agreement with the result $B(b \to \ell) = (10.5 \pm 0.2 \pm 0.3)\%$, measured by CLEO [20] assuming the ACCMM decay model (additional error results from using different decay models). Other measurements of this quantity in Z^0 decays have been performed by L3 [13] and DELPHI [8], although the latter does not include systematic errors due to the modelling of semileptonic decays of b- and c-flavoured hadrons, charm fragmentation and uncertainty in $B(b \to c \to \ell)$.

The measured value of $B(b \to c \to \ell)$ is the first such measurement published for b-flavoured hadrons produced in Z^0 decays. It can be compared with measurements by CLEO [20]. For example, with the ACCMM model they measure

$$B(b \to c \to \ell) + B(b \to \bar{c} \to \ell) = (9.7 \pm 0.8 \pm 0.6)\%.$$

Their values are 9.3% and 11.1% when using the ISGW** and ISGW models, respectively. The branching ratio can be expected to be reduced by the presence of B_s^0 and b-baryons in Z^0 decays, by a factor of about 0.93 [17]. To make a reasonable comparison with the measured value in this paper, the CLEO number is therefore reduced by 7% and the value of 1.3% assumed for $B(b \to \bar{c} \to \ell)$ is subtracted to obtain $(7.7 \pm 0.9 \pm 0.9)\%$. The first error is the combined statistical and systematic error for the ACCMM model, and the second error accounts for the

model dependence. It may be seen that the agreement with the result in this paper is excellent, and that the new result is more precise.

The measurement of $\langle x_E \rangle$ for b-flavoured hadrons is the most precise single measurement from Z^0 decays presented so far, and is in excellent agreement with previous measurements [12, 13, 16, 14]. The result is limited by knowledge of the shape of the fragmentation function.

To summarise, a simultaneous fit was performed to single-lepton and dilepton events selected from the data collected during the 1990 and 1991 runs with the OPAL detector. The following parameters were determined:

$$\begin{aligned} \chi &= 0.143^{+0.022}_{-0.021} \pm 0.007 \\ \Gamma(Z^0 \to b\bar{b})/\Gamma(Z^0 \to \text{hadrons}) &= 0.222 \pm 0.011 \pm 0.007 \\ B(b \to \ell) &= (10.5 \pm 0.6 \pm 0.5)\% \\ B(b \to c \to \ell) &= (7.7 \pm 0.4 \pm 0.7)\% \\ \langle x_E \rangle &= 0.697 \pm 0.006 \pm 0.011 \end{aligned}$$

where the errors are statistical and systematic, respectively. Unlike some earlier results, our result for $B(b \to c \to \ell)$ excludes decays of the type $b \to \bar{c} \to \ell$.

Acknowledgements

It is a pleasure to thank the SL Division for the efficient operation of the LEP accelerator, the precise information on the absolute energy, and their continuing close cooperation with our experimental group. In addition to the support staff at our own institutions we are pleased to acknowledge the
Department of Energy, USA,
National Science Foundation, USA,
Texas National Research Laboratory Commission, USA,
Science and Engineering Research Council, UK,
Natural Sciences and Engineering Research Council, Canada,
Fussefeld Foundation,
Israeli Ministry of Energy and Ministry of Science,
Minerva Gesellschaft,
Japanese Ministry of Education, Science and Culture (the Monbusho) and a grant under the Monbusho International Science Research Program,
German Israeli Bi-national Science Foundation (GIF),
Direction des Sciences de la Matière du Commissariat à l'Energie Atomique, France,
Bundesministerium für Forschung und Technologie, Germany,
National Research Council of Canada,
A.P. Sloan Foundation and Junta Nacional de Investigacão Científica e Tecnológica, Portugal.

References

[1] For a review see:
P.J.Franzini, Physics Reports **173** (1989) 1.

[2] N.Cabibbo, Phys. Rev. Lett. **10** (1963) 531;
M.Kobayashi and T.Maskawa, Prog. Theo. Phys. **49** (1973) 652.

[3] ARGUS Collaboration, H.Albrecht *et al.*, Phys. Lett. **B 192** (1987) 245;
CLEO Collaboration, M.Artuso *et al.*, Phys. Rev. Lett. **62** (1989) 2233.

[4] CLEO Collaboration, J.Bartelt *et al.*, Cornell Report CLNS 93/1207, submitted to Phys. Rev. Lett.

[5] Particle Data Group, K. Hikasa *et al.*, Phys. Rev. **D 45** (1992) S1.

[6] UA1 Collaboration, C.Albajar *et al.*, Phys. Lett. **B 186** (1987) 247;
MAC Collaboration, H.Band *et al.*, Phys. Lett. **B 200** (1988) 221;
MARK II Collaboration, A.J.Weir *et al.*, Phys. Lett. **B 240** (1990) 289;
L3 Collaboration, B.Adeva *et al.*, Phys. Lett. **B 252** (1990) 703;
ALEPH Collaboration, D.Decamp *et al.*, Phys. Lett. **B 258** (1991) 236;
UA1 Collaboration, C.Albajar *et al.*, Phys. Lett. **B 262** (1991) 171;
CDF Collaboration, F.Abe *et al.*, Phys. Rev. Lett. **67** (1991) 3351;
ALEPH Collaboration, D.Buskulic *et al.*, Phys. Lett. **B 284** (1992) 177;
L3 Collaboration, B.Adeva *et al.*, Phys. Lett. **B 288** (1992) 395.

[7] OPAL Collaboration, P. Acton *et al.*, Phys. Lett. **B 276** (1992) 379.

[8] DELPHI Collaboration, P.Abreu *et al.*, Phys. Lett. **B 301** (1993) 145.

[9] The LEP Collaborations, ALEPH, DELPHI, L3 and OPAL, Phys. Lett. **B 276** (1992) 247;
DELPHI Collaboration, P. Abreu *et al.*, Nucl. Phys. **B 367** (1991) 511;
L3 Collaboration, O. Adriani *et al.*, CERN-PPE/93-31, submitted to Phys. Rep.;
ALEPH Collaboration, D. Buskulic *et al.*, CERN-PPE/93-40, submitted to Z. Phys. C.

[10] OPAL Collaboration, P. Acton et al., Z. Phys. **C 58** (1993) 219.

[11] MARK II Collaboration, J.F. Kral *et al.*, Phys. Rev. Lett. **64** (1990) 1211;
L3 Collaboration, B. Adeva *et al.*, Phys. Lett. **B 241** (1990) 416;
OPAL Collaboration, M. Akrawy *et al.*, Phys. Lett. **B 263** (1991) 311;
MARK II Collaboration, R.G. Jacobsen *et al.*, Phys. Rev. Lett. **67** (1991) 3347;
DELPHI Collaboration, P. Abreu *et al.*, Phys. Lett. **B 281** (1992) 383;
DELPHI Collaboration, P. Abreu *et al.*, Phys. Lett. **B 295** (1992) 383;
L3 Collaboration, O. Adriani *et al.*, CERN-PPE/93-60, submitted to Phys. Lett. B.

[12] ALEPH Collaboration, D. Decamp *et al.*, Phys. Lett. **B 244** (1990) 551.

[13] L3 Collaboration, B. Adeva *et al.*, Phys. Lett. **B 261** (1991) 177.

[14] OPAL Collaboration, M. Akrawy *et al.*, Phys. Lett. **B 263** (1991) 311.

[15] OPAL Collaboration, P. Acton *et al.*, Z. Phys. **C 55** (1992) 191.

[16] DELPHI Collaboration, P. Abreu *et al.*, Z. Phys **C 56** (1992) 47.

[17] OPAL Collaboration, P. Acton *et al.*, *Measurement of* $\Gamma(Z^0 \to b\bar{b})/\Gamma(Z^0 \to \text{hadrons})$ *using Leptons*, CERN-PPE/93-46, to be published in Z. Phys. C.

[18] OPAL Collaboration, P. Acton *et al.*, *A measurement of* $\Gamma(Z^0 \to b\bar{b})/\Gamma(Z^0 \to \text{hadrons})$ *using an impact parameter technique*, CERN-PPE/93-79, submitted to Z. Phys. C.

[19] J. L. Cortes *et al.*, Phys. Rev. **D 25** (1982) 188;
F. J. Gilman, in *Proceedings of the Fourteenth SLAC Summer Institute on Particle Physics*, edited by E. Brennan (Stanford, 1986), p. 191;
A.Khodjamirian, S.Rudaz and M.B.Voloshin, Phys. Lett. **B 242** (1990) 489.

[20] CLEO Collaboration, S.Henderson *et al.*, Phys. Rev. **D 45** (1992) 2212.

[21] ARGUS Collaboration, H.Albrecht *et al.*, Phys. Lett. **B 249** (1991) 359.

[22] I.I. Bigi, N.G. Uraltsev and A.I. Vainshtein, Phys. Lett. **B 293** (1992) 430.

[23] OPAL Collaboration, K.Ahmet *et al.*, Nucl. Instr. and Meth. **A 305** (1991) 275.

[24] M.Hauschild *et al.*, Nucl. Instr. and Meth. **A 314** (1992) 74.

[25] J. Allison *et al.*, Nucl. Instr and Meth. **A 317** (1992) 47.

[26] W. Bartel *et al.*, Z. Phys. **C 33** (1986) 23;
S. Bethke *et al.*, Phys. Lett. **B 213** (1988) 235.

[27] OPAL Collaboration, M. Z. Akrawy *et al.*, Z. Phys. **C 49** (1991) 375.

[28] T.Sjöstrand, Comp. Phys. Comm. **39** (1986) 347;
M. Bengtsson and T. Sjöstrand, Comp. Phys. Comm. **43** (1987) 367;
M. Bengtsson and T. Sjöstrand, Nucl. Phys. **B 289** (1987) 810;
T. Sjöstrand, CERN-TH/92-6488.

[29] Parameter values were tuned to describe global event shape variables:
OPAL Collaboration, M. Akrawy *et al.*, Z. Phys. **C 47** (1990) 505.

[30] C.Peterson, D.Schlatter, I.Schmitt and P.M.Zerwas, Phys. Rev. **D 27** (1983) 105.

[31] B.Andersson, G.Gustafson and B.Söderberg, Z. Phys. **C 20** (1983) 317.

[32] D.Bardin et al., *ZFITTER, An Analytical Program for Fermion Pair Production in* e^+e^- *Annihilation*, CERN-TH.6443/92.
For this prediction, the Z^0, top quark, and Higgs boson masses are $M_Z = 91.18$ GeV/c^2, $M_{\text{top}} = 150$ GeV/c^2 and $M_{\text{Higgs}} = 300$ GeV/c^2, and $\alpha_s = 0.12$.

[33] G. Altarelli *et al.*, Nucl. Phys. **B 208** (1982) 365.

[34] N.Isgur, D.Scora, B.Grinstein and M.Wise, Phys. Rev. **D 39** (1989) 799.

[35] DELCO Collaboration, W. Bacino *et al.*, Phys. Rev. Lett. **43** (1979) 1073.

[36] CLEO Collaboration, D. Bortoletto *et al.*, Phys. Rev. **D 45** (1992) 21.

[37] OPAL Collaboration, G. Alexander et al., Phys. Lett. **B 262** (1991) 341.

[38] P.Collins and T.Spiller, J. Phys. **G 11** (1985) 1289;
V.G.Kartvelishvili, A.K.Likhoded and V.A.Petrov, Phys. Lett. **B 78** (1978) 615.
M.G.Bowler, Z. Phys. **C 11** (1981) 169;
D.A.Morris, Nucl. Phys. **B 313** (1989) 634;
and see *Heavy Flavours* in Z Physics at LEP1, CERN 89-08, ed. G. Altarelli *et al.*, Vol. 1 (1989) 267.

[39] T.Mannel and G.Schuler, Phys. Lett. **B 279** (1992) 194.

[40] ARGUS Collaboration, H. Albrecht *et al.*, DESY 92-029;
CLEO Collaboration, R. Fulton *et al.*, Phys. Rev. **D 43** (1991) 651.

[41] ARGUS Collaboration, H. Albrecht *et al.*, DESY 92-146.

[42] Assuming relative production rates during fragmentation for $u\bar{u} : d\bar{d} : s\bar{s}$: diquarks of $1.0 : 1.0 : 0.3 : 0.23$, consistent with the measured yield of hadrons of various flavours in e^+e^- annihilation at lower energies and at LEP, gives production ratios of 39.5% B_d, 39.5% B_u, 12% B_s and 9% b-flavoured baryon.
For the $s\bar{s}$ fraction at LEP see:
OPAL Collaboration, G.Alexander *et al.*, Phys. Lett. **B 264** (1991) 467;
DELPHI Collaboration, P.Abreu *et al.*, Phys. Lett. **B 275** (1992) 231.
For reviews see:
T. Sjöstrand *et al.*, in Z physics at LEP 1, ed. G.Altarelli *et al.*,
CERN 89-08, Vol 3 (1989) 143;
D.H. Saxon, *Quark and Gluon Fragmentation in High Energy* e^+e^- *Annihilation*,
RAL-86-057.

Figure Captions

Figure 1: The distributions for electron candidates, with no transverse momentum requirements, of
a) $N^{\sigma}_{E_{\rm cone}/p}$ for $p < 6$ GeV/c;
b) $N^{\sigma}_{{\rm d}E/{\rm d}x}$ for $p < 6$ GeV/c;
c) $N^{\sigma}_{E_{\rm cone}/p}$ for $p > 6$ GeV/c;
d) $N^{\sigma}_{{\rm d}E/{\rm d}x}$ for $p > 6$ GeV/c.
In this context, the electron candidates have satisfied all requirements except in the distribution displayed. The arrows indicate the selection requirements in the electron identification procedure, and the solid histogram is the fitted background contribution as described in Section 4. For the ${\rm d}E/{\rm d}x$ fits, the fitted total of background and signal is indicated by the dashed line. The signal region was excluded in the $E_{\rm cone}/p$ fits.

Figure 2: The distribution of $N^{\sigma}_{E_{\rm cone}/p}$ for electron candidates, integrated over all p and $p_{\rm T}$ bins. The distribution from the data is shown in (a), with the fitted background contribution shown by the solid line. The equivalent distribution from Monte Carlo events is shown in (b) with the fitted background contribution and the known non-electrons indicated.

Figure 3: The fitted p versus $p_{\rm T}$ distributions for single leptons. For clarity, the projections of the two-dimensional distributions are shown in
a) for muon $p_{\rm T}$ with $p > 5$ GeV/c;
b) for muon p with $p_{\rm T} > 1.2$ GeV/c;
c) for electron $p_{\rm T}$ with $p > 2$ GeV/c;
d) for electron p with $p_{\rm T} > 1.2$ GeV/c.
The arrows indicate the minimum values of p and $p_{\rm T}$ used in the fit. In the muon case, the selection was the logical "OR" of the regions indicated by the solid and the dashed arrows. The contributions after the fit from the different processes are indicated. Primary b includes $\rm b \to \ell$ and $\rm b \to \tau \to \ell$ decays. Secondary b includes $\rm b \to c \to \ell$, $\rm b \to \bar{c} \to \ell$ and $\rm b \to J/\psi \to \ell\ell$ decays. The primary c component contains $\rm c \to \ell$ decays in $\rm Z^0 \to c\bar{c}$ events.

Figure 4: The distributions of $p^{\rm max}_{\rm comb}$ versus $p^{\rm min}_{\rm comb}$ for opposite-jet dilepton events. The contributions are indicated from events where both leptons are from $\rm b \to \ell$ decays, where one lepton is from $\rm b \to \ell$ decay and the other from $\rm b \to c \to \ell$, where both are from $\rm b \to c \to \ell$ decays, and where both are from $\rm c \to \ell$ decays.

Figure 5: Distributions of $p^{\rm min}_{\rm comb}$ for pairs of leptons separated by at least 60°, shown separately for $\mu\mu$ events, eμ events, ee events and the sum of the three channels, with the fitted contributions superimposed. The arrows indicate the minimum values of $p^{\rm min}_{\rm comb}$ used in the fit. The primary b component contains events where both leptons are from $\rm b \to \ell$ or $\rm b \to \tau \to \ell$ decay. The secondary b component contains events with at least one lepton from $\rm b \to c \to \ell$, $\rm b \to \bar{c} \to \ell$ or $\rm b \to J/\psi \to \ell\ell$ decay. The second lepton candidate may be a prompt lepton from any source. The primary c contribution contains $\rm Z^0 \to c\bar{c}$ events with both leptons from $\rm c \to \ell$ decays.

Figure 6: The fraction, R, of the number of opposite-jet dilepton events that are same-sign versus $p^{\rm min}_{\rm comb}$, shown separately for $\mu\mu$ events, eμ events, ee events and the sum of the

three channels. The fitted distribution is superimposed, together with the prediction for $\chi = 0$. The arrows indicate the minimum values of $p_{\rm comb}^{\rm min}$ used in the fit.

Figure 7: Distributions of m_{ll} for pairs of leptons closer than 60°, shown separately for opposite-sign and same-sign $\mu\mu$, eμ and ee events, with the fitted contributions superimposed. The arrows indicate the minimum values of m_{ll} used in the fit. The secondary b component in this case contains events where one lepton is from b $\to \ell$ or b $\to \tau \to \ell$ decay, and the other is from b $\to$ c $\to \ell$ decay. The same-sign events test the estimates of non-prompt background.

Figure 8: The $\rm B_s^0$ mixing parameter, $\chi_{\rm s}$, versus $f_{\rm s},$. the fraction of b-flavoured hadrons in semileptonic decays that are $\rm B_s^0$ mesons. The line is obtained by combining the OPAL measurement with measurements of $\rm B_d^0$ mixing from CLEO [4]. The dashed lines indicate the one-standard-deviation errors.

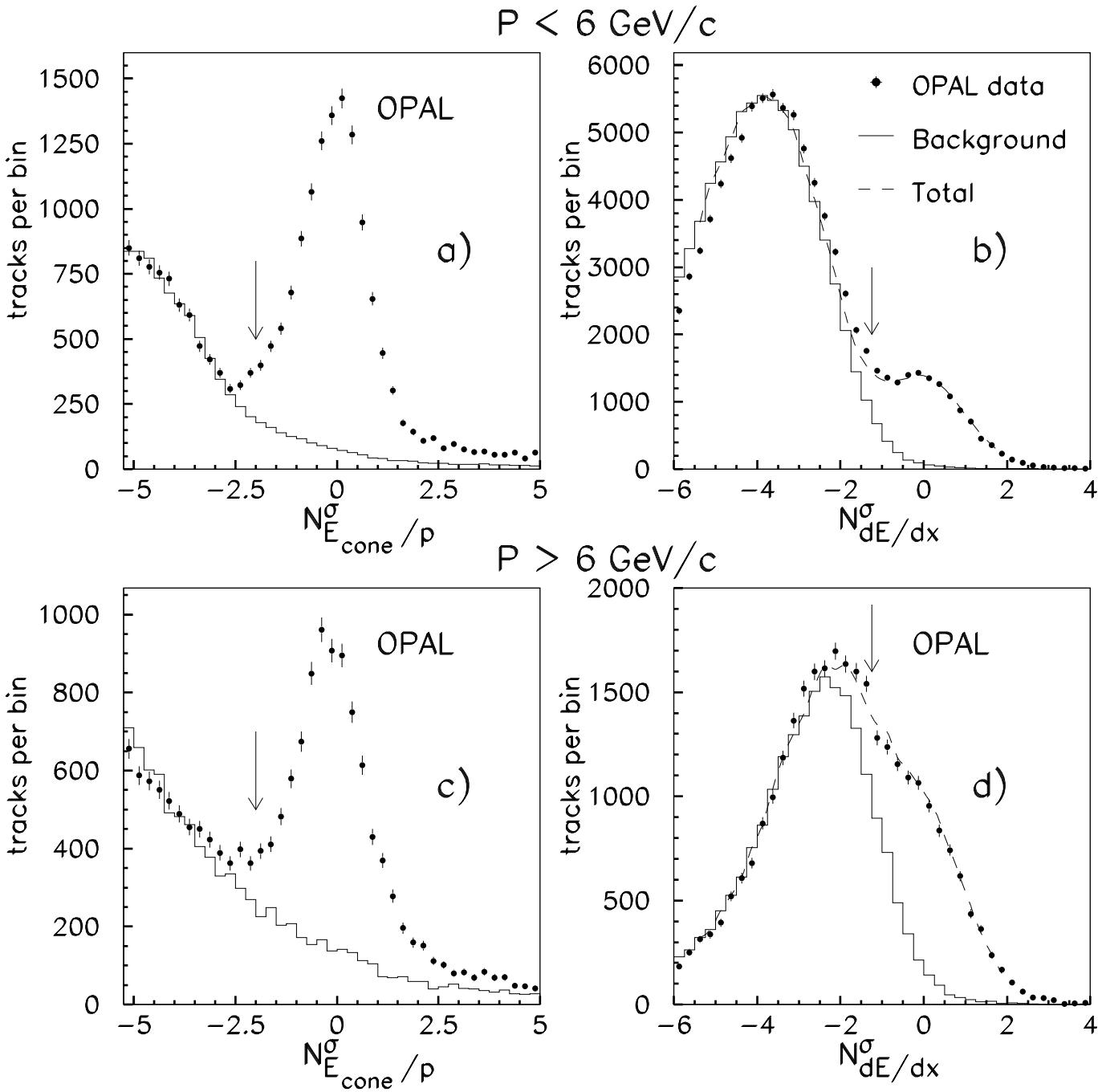
P < 6 GeV/c
OPAL
a)
tracks per bin
$N^{\sigma}_{E_{cone}/p}$
OPAL data
Background
Total
b)
$N^{\sigma}_{dE/dx}$
P > 6 GeV/c
c)
d)

Figure 1

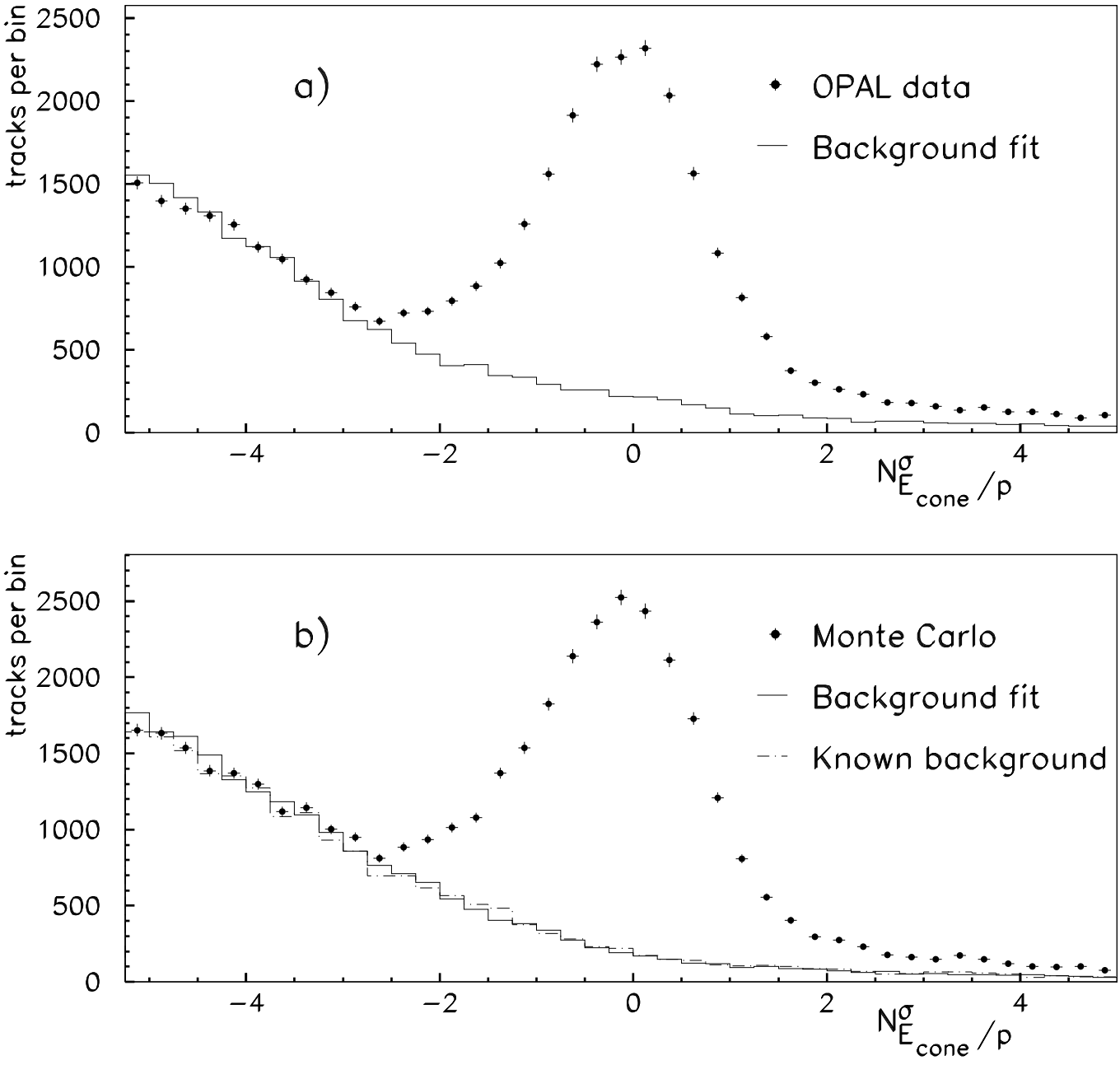
a)
OPAL data
Background fit
tracks per bin
2500
2000
1500
1000
500
0
−4
−2
0
2
4
$N^{\sigma}_{E_{cone}}/p$
b)
Monte Carlo
Background fit
Known background
tracks per bin
2500
2000
1500
1000
500
0
−4
−2
0
2
4
$N^{\sigma}_{E_{cone}}/p$

Figure 2

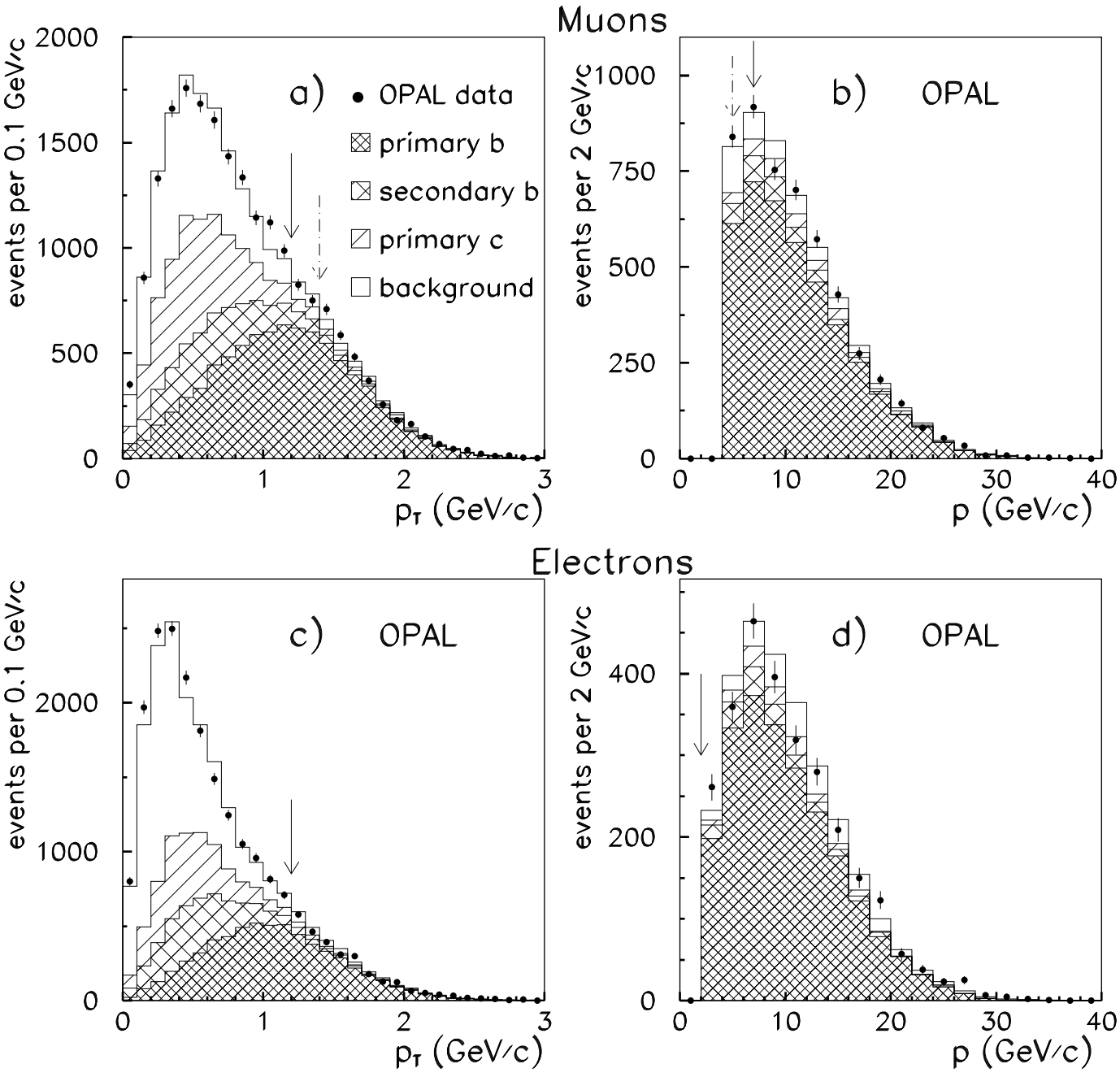
Muons
a)
OPAL data
primary b
secondary b
primary c
background
events per 0.1 GeV/c
p_T (GeV/c)
b)
OPAL
events per 2 GeV/c
p (GeV/c)
Electrons
c)
OPAL
events per 0.1 GeV/c
p_T (GeV/c)
d)
OPAL
events per 2 GeV/c
p (GeV/c)

Figure 3

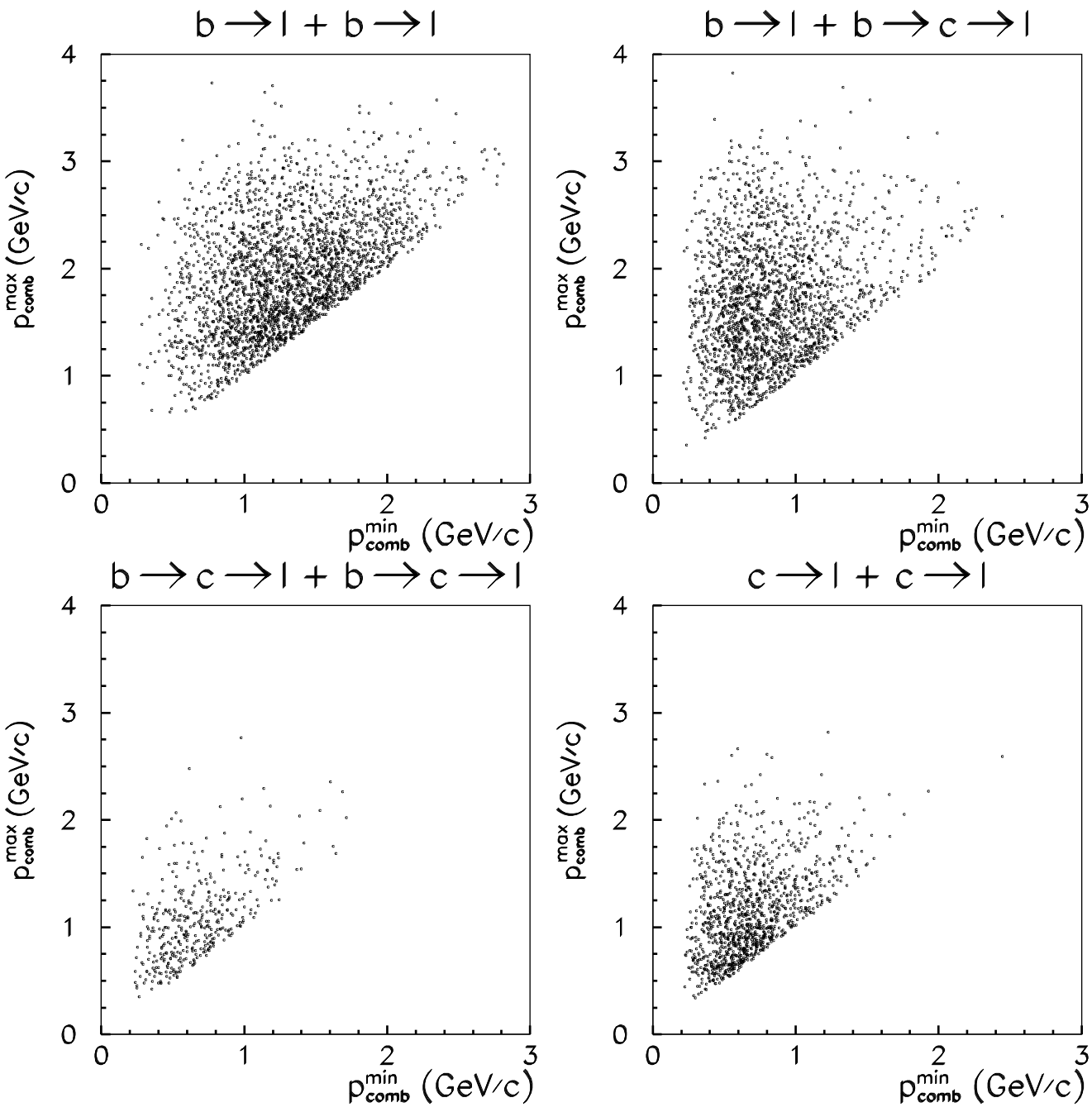

Figure 4

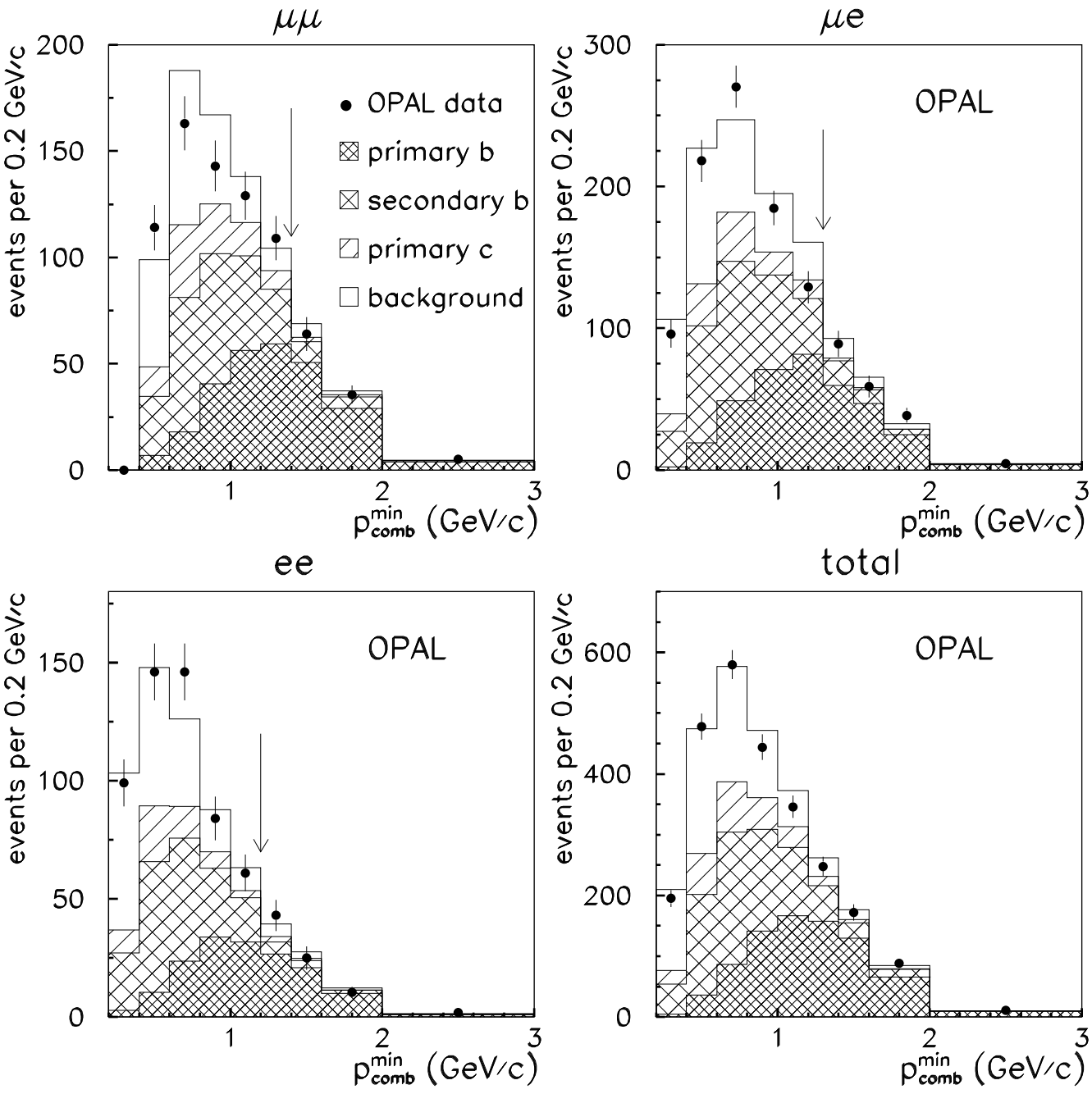
μμ
μe
ee
total
OPAL data
primary b
secondary b
primary c
background
OPAL
events per 0.2 GeV/c
p^{min}_{comb} (GeV/c)

Figure 5

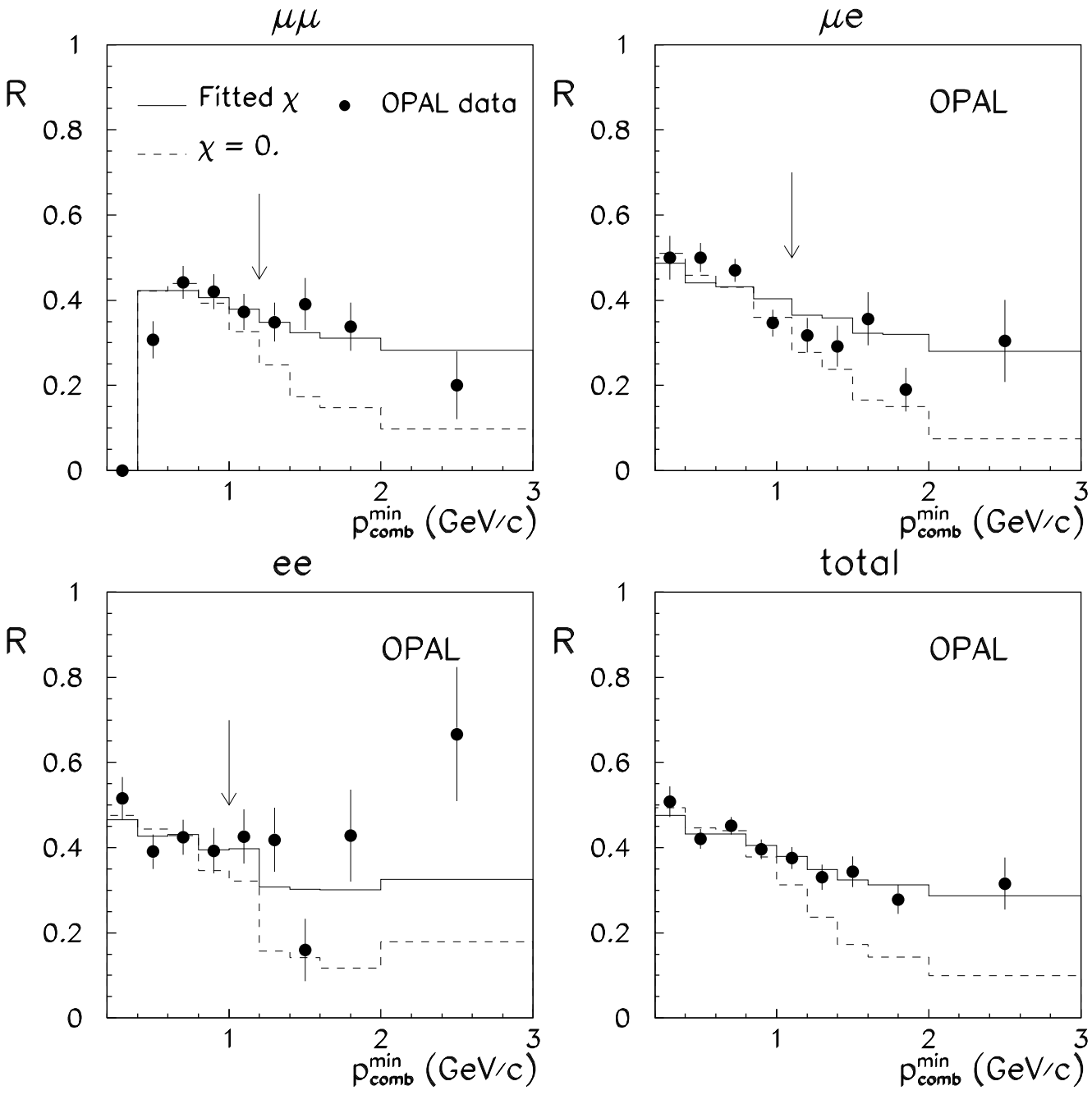

Figure 6

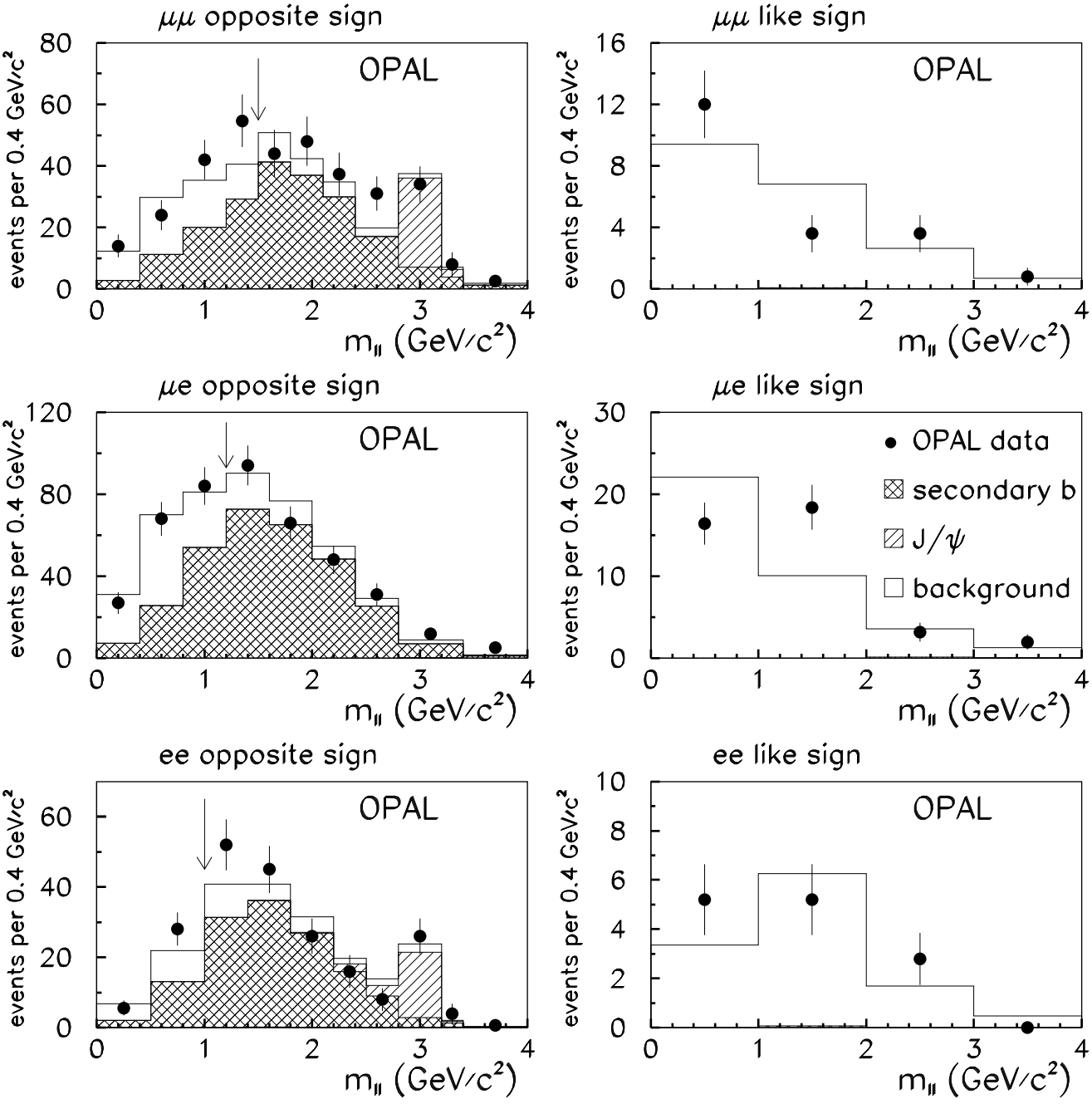
μμ opposite sign
μμ like sign
μe opposite sign
μe like sign
ee opposite sign
ee like sign
OPAL
OPAL data
secondary b
J/ψ
background
events per 0.4 GeV/c²
m_ll (GeV/c²)

Figure 7

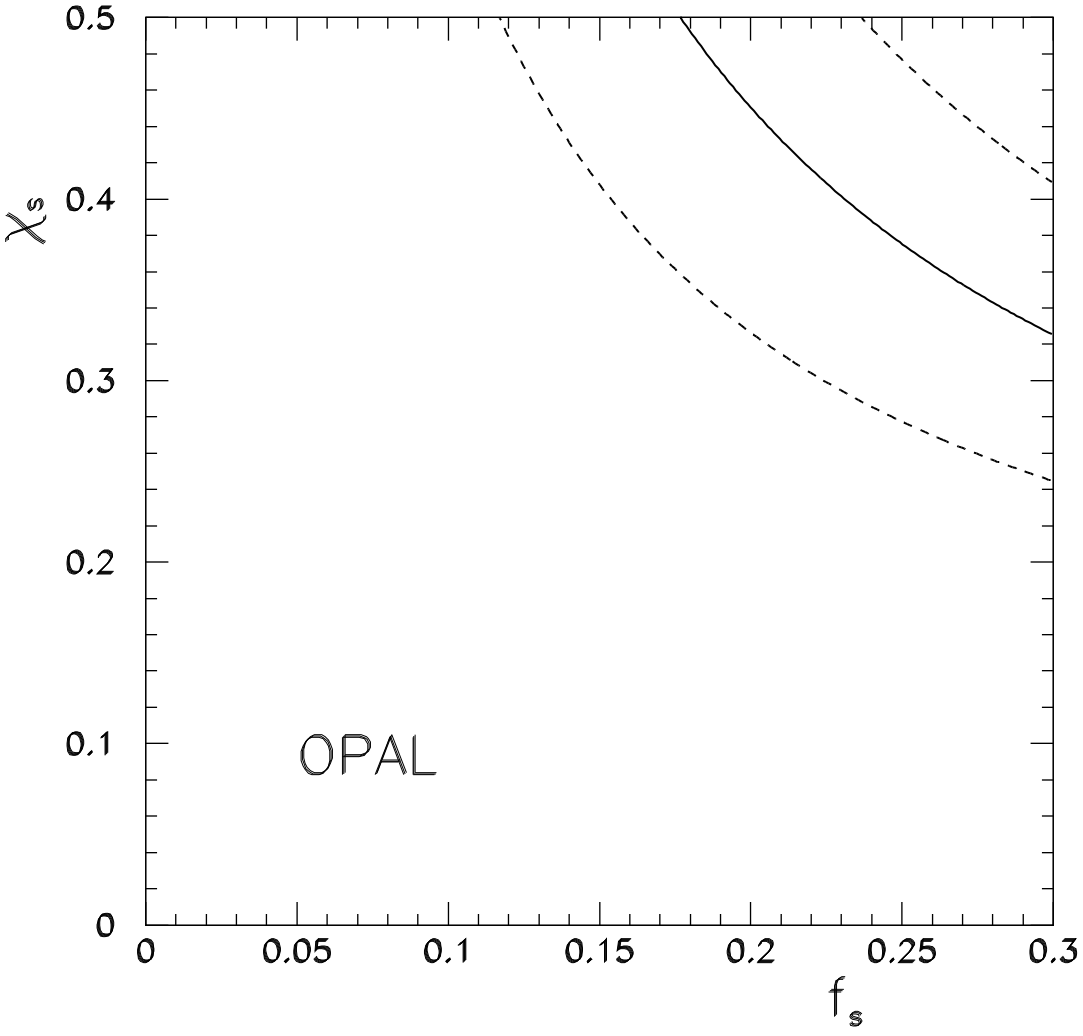

Figure 8